Proceedings of UGSAS-GU & BWEL Joint Poster Presentation on Agricultural and Basin Water Environmental Sciences 2023

Date: November 8, 2023
Venue: UGSAS-GU Building 6F Main Seminar Room

Organized by
The United Graduate School of Agricultural Science, Gifu University (UGSAS-GU).
Gifu University Rearing Program for Basin Water Environmental Leaders (BWEL).

Co-organized by
International Consortium of Universities in South and Southeast Asia for the Doctoral Education in Agricultural Science and Biotechnology (IC-GU12).

Table of Contents

Behavior and Welfare of Japanese Black Cattle During Transportation Activities

Gianne Bianca P. Manalo[1] and Shigeru Ninomiya[2]

[1] The United Graduate School of Agricultural Science, Gifu University, 1-1 Yanagido, Gifu-shi, Gifu 501-1193, Japan
[2] Faculty of Applied Biological Sciences, Gifu University, 1-1 Yanagido, Gifu-shi, Gifu 501-1193, Japan

INTRODUCTION

Pre-slaughter management of beef cattle is a critical phase in beef production that involves preparing cattle for the journey to the processing facility or slaughterhouse. Proper pre-slaughter management entails strict adherence to regulatory protocols and requirements established by authorities to ensure meat quality and food safety while upholding animal welfare. Despite optimal conditions, pre-slaughter activities such as transportation can inflict injuries, pain, fear, and suffering on animals (Özdemir et al., 2022). Animals are compelled to cope with these challenges through their behavioral and physiological responses (Day and Stull, 1997). Although transportation is a relatively brief phase in beef cattle production, it can be challenging to manage due to its detrimental impact on animal welfare.

The primary objective of this study is to compare the effects of two transportation methods on the behavior and welfare of Japanese Black Cattle. Investigating the transportation method is crucial because the process of moving animals to the slaughter facility influences the stress levels of cattle during exsanguination (Özdemir et al., 2022). By assessing their behavior and welfare, researchers can determine which mode of transportation can minimize stress in cattle during this critical period. Furthermore, studying cattle behavior in slaughterhouses will guide researchers in identifying areas where experimental research is needed and will provide a preliminary assessment of animal welfare (Moss, 1984).

Influential factor during pre-slaughter stage

Several influential factors before the pre-slaughter stage of beef cattle play a pivotal role in ensuring animal welfare, meat quality, and food safety. A previous study by Wibowo et al. (2022) revealed that the incidence of falling animals during pre-slaughter activities was approximately 6.3%, exceeding the animal welfare standards set for Samari, Indonesia, which should be 1% or less. Poor handling is one of the contributing factors that induces stress in beef cattle, making them more aggressive, averse, and agitated, thereby making them difficult to manage during the pre-slaughter phase. Several management considerations, including but not limited to feed withdrawal, water supply, health assessment, rest and adaptation, facility maintenance, vehicle design, temperature, ventilation, and other environmental factors, are strongly linked to the occurrence of falling animals during pre-slaughter handling (Grandin, 2017).

Animal behavior during the pre-slaughter phase is significantly influenced by animal-human interactions at an earlier stage in their lives. Consequently, cattle's fear of humans can impact their well-being and potentially compromise meat quality. Conversely, animals that have experienced good stockmanship may be less prone to this issue, as they are accustomed to being handled prior to the slaughtering procedure (Njisane and Muchenje, 2017). Therefore, farm personnel play a crucial role before the slaughtering process, responsible for reducing the animal's aggression and promoting calmness throughout this phase.

Transportation Stressors

Previous studies have examined both the duration and quality of transportation for animals intended for meat production (González et al., 2012; Nielsen et al., 2011). They discovered that during transportation, shrinkage is a significant economic factor. Moreover, Miranda-de la Lama et al., (2012) emphasize that transportation was the link of all the process prior to slaughtering of cattle. Researchers also noted that factors such as speed, vehicle design (size, space, and surface), and stocking density can induce pre-slaughter stress. Inadequate management and a lack of control over the animal's external environment may lead to abnormal behavior, as animals attempt to cope through physiological changes (Broom, 2015). Slaughter facilities present a new environment and experience for the animals, requiring adjustments in their behavior and physiology. Some studies have reported that age, gender, species, and breed play crucial roles in how animals respond to stress.

The duration of transportation is one of the most extensively studied stressors, although some research has focused on transport distance (Eldridge and Winfield, 1988; Wythes et al., 1981). Studies indicate that extended hours of transport can increase the risk of water and tissue loss, deplete energy reserves, and result in dehydration and fatigue (Schwartzkopf-Genswein et al., 2012). Moreover, unfavorable conditions are not solely dependent on transport duration and distance; factors such as loading and unloading, the number of stops during transport, driving style, and the interior design of the transport vehicle also contribute to the stress experienced by the animals (Dalla Villa et al., 2009).

In addition to ambient temperature, various environmental factors, such as relative humidity (RH),

solar radiation, surrounding temperature, heat and moisture produced by animals, heat loss from the vehicle, microclimatic factors interact with each other and should be considered when assessing animal welfare during transportation activities. Furthermore, animals with aggressive, active, and fearful behaviors require different handling approaches.

The age and breed of the animals must also be taken into account when determining their diet, appropriate length of rest periods, and the selection of bedding materials. Animal behavior is often significantly influenced by their breed and temperament, which can also impact the incidence of bruising during transportation activities. The presence or absence of horns, skin texture, thickness, and other behavioral traits vary among breeds. As a result, transport-related injuries and bruising experienced by animals intended for meat production also depend on these factors.

Effect of transportation stress on animal's physiology and welfare

Stress can have a negative impact on an animal's physiology and welfare, potentially leading to the release of stress hormones, including cortisol. In fact, a previous study reported that pre-slaughter stress during transport can influence the immune system of cattle (Hulbert et al., 2011). Prolonged elevation of stress hormones, particularly during transportation activities, can result in a weakened immune system, impaired metabolism, and various health issues.

A previous study reported that during the early phase of transportation, cattle exhibit higher levels of socializing and altered behavior (Swanson and Morrow-Tesch, 2001). In a study by Kent and Ewbank (1986), older calves spent less time ruminating and lying and excreted more compared to younger calves, indicating that transportation activities are more stressful for them. On the other hand, Deters and Hansen (2022) reported that road-transported steers had a greater increase in the neutrophil-to-lymphocyte ratio and serum nonesterified fatty acids, indicating a stronger inflammatory and neuroendocrine response compared to steers that were not transported.

REFERENCES

Broom, DM and Fraser AF (2015) Domestic Animal Behaviour and Welfare. Vol. 5.

Dalla Villa PD, Marahrens M, Calvo AV, Di Nardo A, Kleinschmidt N, Alvarez CF and Müller-Graf C (2009) Project to develop animal welfare risk assessment guidelines on transport. EFSA Supporting Publications, 6(9), 21E.

Day F and Stull CL (1997) Stress and Dairy Calves.

Deters EL and Hansen SL (2022) Long-distance transit alters liver and skeletal muscle physiology of beef cattle. Animal, 16(6).

Eldridge GA and Winfield CG (1988) The behaviour and bruising of cattle during transport at different space allowances. Aust. J. Exp. Agric., 28(6): 695–698.

González LA, Schwartzkopf-Genswein KS, Bryan M, Silasi R and Brown F (2012) Space allowance during commercial long distance transport of cattle in North America 1. J. Anim. Sci, 90: 3618–3629.

Grandin T (2017) On-farm conditions that compromise animal welfare that can be monitored at the slaughter plant. Meat Sci. 132: 52–58.

Hulbert LE, Carroll JA, Burdick NC, Randel RD, Brown MS and Ballou MA (2011) Innate immune responses of temperamental and calm cattle after transportation. Vet. Immunol. Immunopathol., 143(1–2): 66–74.

Kent JE and R Ewbank (1986) The effect of road transportation on the blood constituents and behaviour of calves. I. Three months old. Br. Vet. J., 142: 326–335.

Miranda-de la Lama GC, Leyva IG, Barreras-Serrano A, Pérez-Linares C, Sánchez-López E, María GA and Figueroa-Saavedra F (2012) Assessment of cattle welfare at a commercial slaughter plant in the northwest of Mexico. Trop Anim Health Prod., 44(3), 497–504.

Moss R (1984) Observation before experimentation monitoring animal/environment interaction. In Proceedings of the International Congress on Applied Ethology in Farm Animals, pp. 378–381.

Nielsen BL, Dybkjr L and Herskin MS (2011) Road transport of farm animals: Effects of journey duration on animal welfare. Animal, 5(3): 415–427.

Njisane YZ and Muchenje V (2017) Farm to abattoir conditions, animal factors and their subsequent effects on cattle behavioural responses and beef quality - A review. Asian-australas. J. Anim. Sci., 30(6): 755–764.

Özdemir S, Ekiz EE and Ekiz B. (2022) Effect of lairage duration on cattle behaviors and stockperson actions in the slaughter corridor in Simmental and Swiss Brown breeds. Trop Anim Health Prod ., 54(2): 139.

Schwartzkopf-Genswein KS, Faucitano L., Dadgar S, Shand P, González LA and Crowe TG (2012) Road transport of cattle, swine and poultry in North America and its impact on animal welfare, carcass and meat quality: A review. Meat Sci. 92(3): 227–243.

Swanson JC and Morrow-Tesch J (2001) Cattle transport: Historical, research, and future perspectives. J. Anim. Sci., 79: E102–E109.

Wibowo A, Ardhani F, Safitri A, Suhardi S, Inestika V, Anindyasari D and Indana K. (2022). The Impact of Pre-Slaughter and Slaughter Procedure on Animal Welfare and Behavior Changes in Cattle at Local Abattoir in Samarinda-Indonesia. In International Conference on Tropical Agrifood, Feed and Fuel (ICTAFF 2021). Adv. Biol. Res. Atlantis Press. 17: 236–239.

Wythes J R, Arthur RJ, Thompson PJM, Williams GE and Bond JH (1981) Effects of transporting cows various distances on liveweight, carcase traits and muscle pH. Aust. J. Exp. Agric. 21(113): 557–561.

Comparing the Prediction Performance, Extrapolation Potential of Different Algorithms While Using Fourier Transform Infrared Spectroscopy of Soil

He Jingyun, Matsui Tsutomu and Tanaka S. T. Takashi

The United Graduate School of Agricultural Science, Gifu University, 1-1 Yanagido, Gifu-shi, Gifu 501-1193, Japan

INTRODUCTION

Precision agriculture (PA) is the application of technologies and principles to manage the spatial variability associated with all aspects of agricultural production to improve crop performance and environmental quality (Carrer et al., 2022; Zhang et al., 2002). Soil physical, hydrological, chemical, and biological features are key knowledge for understanding the relationships between soil and crops, especially in PA, environmental management, and crop growth modeling (Bhakta et al., 2019). In recent years, spectroscopy has attracted great attentions as it is a non-destructive and more time-saving analytical tool that can simultaneously analyze various soil properties based on specific peaks. Combining Fourier Transform Infrared Spectroscopy (FTIR) and multivariate regression analysis is a viable alternative to traditional chemical analysis methods. FTIR technology can effectively estimate the target soil properties, such as pH, soil organic carbon (SOC), nitrogen (N), phosphorus (P), potassium (K) and cation exchange capacity (CEC), etc. (Peltre et al., 2014).

A majority of existing experiments predominantly entail the analysis of data acquired from various areas. In interpolation predictions are made using data coming from all geographic directions, while in extrapolation predictions are based on data from one or a few directions only, possibly from far away (Angelini et al., 2020). In the contexts of both interpolation and extrapolation, the utilization of ill-suited models may result in diminished precision of the outcomes. A study states that deterioration of performance when simple interpolation is replaced by simple extrapolation. The potential decrease in accuracy when employing RF for extrapolation purposes remains unclear. (Takoutsing et al., 2020). Thus, we evaluated the aptitude of two specific algorithms, namely Partial Least Squares Regression (PLSR) and Random Forest (RF), with regard to their suitability for either of interpolation or extrapolation task.

MATERIALS AND METHODS

A total of 2,890 soil samples were collected from various regions (e.g., Gifu, Nara, Akita, Hyogo) in Japan, since 2017. pH and Mineralizable Nitrogen (Min N) were measured. Mid-infrared spectroscopy (wavenumber of 4000–500 cm^{-1}) was obtained at the intervals of $4cm^{-1}$ using FTIR analytical instruments coupled with the diffuse reflectance unit (FT/IR-4700, JASCO Company, Japan).

Pre-treatment: When the wavelength is under 500, the raw data were so noisy that we compared two methods for each soil property, including the wavelength under 500 (within noise) and removing the wavelength under 500 (without noise). Three spectral transformation methods including non-order differential (NOD), first-order differential (FOD), and second-order differential (SOD) were compared to select the appropriate number of differentiations according to RMSE values. Thus, the best combination of optimal regression method and differential times were evaluated. Our results conclusively demonstrated that the " NOD with the without noise " yielded superior results for all sampled data.

Two distinct test dataset configurations were implemented: Test 1 - Leave-one-prefecture-out Cross-Validation (LOPO CV) for extrapolation; Test 2 - Random Cross-Validation (Random CV) for interpolation. All algorithms implemented in R. RMSE (Root Mean Squared Error), RRMSE (Relative Root Mean Squared Error), R^2, and LCCC (Lin's Concordance Correlation Coefficient) were evaluated.

RESULTS

In this case, the pH model consistently demonstrated strong performance, even when subjected to LOPO CV(Table 1). This resilience suggests that pH predictions are relatively insensitive to variations in sample origins. In contrast, the model for Min N exhibited enhanced performance during Random CV, underscoring the importance of localized optimization for accurate Min N predictions.

DISCUSSION

Our analysis was limited to two soil properties, and in-depth discussions concerning correlations were constrained. Further research is needed to encompass an array of other soil properties and explore their correlations. Additionally, we will explore the viability

of substituting the soil testing process for the remaining soil properties with FTIR.

	PLSR		RF	
	pH	Min N	pH	Min N
RMSE_T1	0.291	4.527	0.197	2.356
RMSE_T2	0.299	4.349	0.282	3.944
RRMSE_T1	6.598	7.059	4.476	3.674
RRMSE_T2	6.788	6.780	6.389	6.149
R^2_T1	0.465	-0.013	0.678	0.401
R^2_T2	0.373	0.730	0.057	0.699
LCCC_T1	0.794	0.454	0.895	0.781
LCCC _T2	0.724	0.878	0.703	0.886

Table. 1: Comparison model results. (T1: LOPO, T2: Random CV, Min N: Mineralizable Nitrogen)

ACKNOWLEDGMENTS

The analysis of soil samples was conducted using the FTIR and ICP-AES of the Division of Instrument Analysis, Gifu University.

REFERENCES

Carrer, M J, de Souza Filho H M, Vinholis M D M B and Mozambani C I (2022) Precision agriculture adoption and technical efficiency: An analysis of sugarcane farms in Brazil. Technol. Forecast. Soc. Change., 177: 121510.

Zhang N, Wang M and Wang N (2002) Precision agriculture—a worldwide overview. Comput. Electron. Agric. 36(2-3): 113-132.

Bhakta I, Phadikar S and Majumder K (2019) State-of-the-art technologies in precision agriculture: a systematic review. J. Sci. Food Agric., 99(11): 4878-4888.

Peltre C, Bruun S, Du C, Thomsen IK and Jensen LS (2014) Assessing soil constituents and labile soil organic carbon by mid-infrared photoacoustic spectroscopy. Soil Biol. Biochem., 77: 41-50.

Angelini ME, Kempen B, Heuvelink GBM, Temme AJ and Ransom MD (2020) Extrapolation of a structural equation model for digital soil mapping. Geoderma, 367: 114226.

Takoutsing B, Heuvelink GB, Stoorvogel JJ, Shepherd KD and Aynekulu E (2022) Accounting for analytical and proximal soil sensing errors in digital soil mapping. European Journal of Soil Science, 73(2): e13226.

Microbial Fuel Cell and Macropores Play Crucial Roles in Suppressing Nitrous Oxide Emissions from Rice Paddy Fields

Adhia Azhar Fauzan[1], Ken Hiramatsu[1], Takeo Onishi[1] and Tomohiro Egusa[3]

[1] The United Graduate School of Agricultural Science, Gifu University, 1-1 Yanagido, Gifu-shi, Gifu 501-1193, Japan
[2] Faculty of Agriculture, Shizuoka University, 836 Ohya, Suruga-ku, Shizuoka 422-8529, Japan

INTRODUCTION

In the wake of alarming climate reports, including the sobering declaration by the United Nations Secretary-General that 'The era of global warming has ended; the era of global boiling has arrived,' our planet faces an unprecedented climate crisis. The signs are unmistakable– sea ice has reached record lows, global sea surface temperatures continue to break records, and the relentless increase in temperatures is unequivocally linked to heat-trapping greenhouse gases.

Among these greenhouse gases, nitrogen oxide (N_2O) emerges as a significant contributor, despite its seemingly modest percentage in the overall greenhouse gas inventory. N_2O, with a Global Warming Potential (GWP) of 273 times that of carbon dioxide (CO_2), holds the dubious distinction of having the highest GWP.

Agriculture, an industry vital to our survival, is a surprising source of greenhouse gas emissions, responsible for 10% of all emissions. Just like humans, plants need to 'breathe' and, in doing so, release gases that further exacerbate the issue. But here's a twist – only 30% of the fertilizers we use are effectively absorbed by these plants, while the rest finds its way into groundwater or evaporates into more N_2O, aggravating the problem.

Despite our best intentions, the approaches we've taken to combat these greenhouse gas emissions have been flawed, primarily focusing on physical and chemical methods, overlooking a hidden factor that has been right under our feet – microbes. These tiny organisms play a pivotal role in the greenhouse gas equation, consuming plant root exudates, generating electrons as they metabolize them. To complete this process, they require nitrates (NO^{3-}) as electron acceptors, ultimately releasing N_2O gas into the atmosphere.

However, there is hope on the horizon. The journey to address global energy challenges and reduce our dependence on fossil fuels, which began with the advent of Microbial Fuel Cells (MFC) (Davis and Yarbrough 1962), has evolved into a clean and environmentally friendly energy source, aligning with the goals of sustainable development. A combination of MFC and plants offers a novel solution to regulate redox potential (EH) and reduce greenhouse gas emissions. Plant-Microbial Fuel Cells (PMFCs) introduce artificial electron acceptors, preventing the utilization of natural oxidants by microbes, while the remaining oxidants in the soil serve as vital nutrients for plants (Insam and Wett 2008).

The potential of PMFCs in mitigating greenhouse gas emissions, particularly the notorious N_2O, is a promising avenue yet to be fully explored. Moreover, the role of macropores in the soil, another overlooked factor, shows promise in reducing N_2O emissions. Surprisingly, the idea of combining PMFCs and macropores to address N_2O emissions remains uncharted territory, offering a new frontier in the fight against climate change.

This study aimed to examine the emission of N_2O, redox, TOC (Total Organic Carbon) in water, TN (Total Nitrogen) in soil, microbial, as well as plant growth. These observations were made by implementing MFC, macropore, or a combination of both methods. In this exploration, we delve into the uncharted territory of PMFCs, plants, and macropores, seeking to unlock their potential in reducing N_2O emissions—a pursuit critical in our quest to address climate change and preserve the planet for future generations.

MATERIALS AND METHODS

The Research Period spanned from June 19th to September 13th, 2023, allowing for comprehensive data collection and analysis across the designated parameters. GHG Analysis involved the use of a static closed chamber method. Gas samples were collected at 4 PM every week, capturing measurements at five time points (0, 15, 30, 45, and 60 minutes after chamber closure). Gas concentration was determined using a GC 2014, allowing for the calculation of gas flux. Redox Measurement was continuously monitored with a Hioki LR5041, recording data at 5-minute intervals. Electrodes were strategically placed at a depth of 10 cm near the plant roots. Soil Sampling was performed on a weekly basis to collect samples for total nitrogen (N) analysis. Additionally, at the time of harvest, soil samples were gathered for subsequent microbial analysis. Water Sampling involved the collection of water samples from a depth of 20 cm below the soil surface using a Daiki DIK-8392. The Total Organic Carbon (TOC) content in the water samples was determined through analysis with a TOC-V. Plant Data Collection included the regular recording of plant height measurements on a weekly basis throughout the research period. During the harvest, plants were collected for nitrogen level analysis, and the weight of 1000 seeds was determined.

RESULTS AND DISCUSSION

Increasing redox, leading to a positive value, can be interpreted as a success in efforts to reduce N_2O emissions. This is because, in general, redox in flooded

rice fields is in the negative range. The research results indicate that the MFC+MP treatment achieved consistently high redox values over an extended period. However, it's worth noting that this treatment also exhibited higher inconsistency. On the other hand, while the MFC treatment didn't reach the same high values as the MFC+MP treatment, the results tended to be more stable, with consistently positive values. While both MFC and macropore treatments can individually increase redox values, the results of this research lead to the conclusion that their combination does not yield improved results. In fact, it leads to fluctuations.

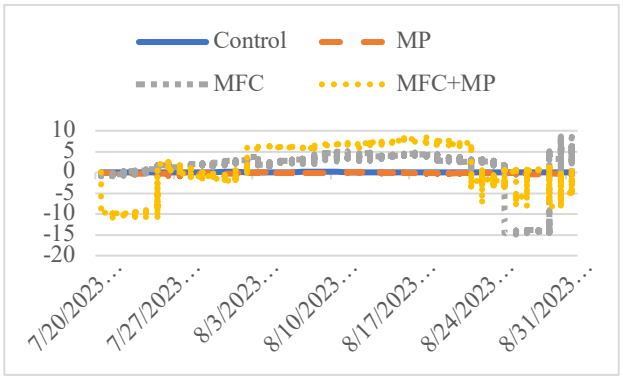

Fig. 1: Redox during the research

The concentration data produced in this study indicates that the MFC treatment has the lowest concentration, while the control group emits higher N_2O concentrations. This observation can be deduced from the redox results, which lead to the following outcomes.

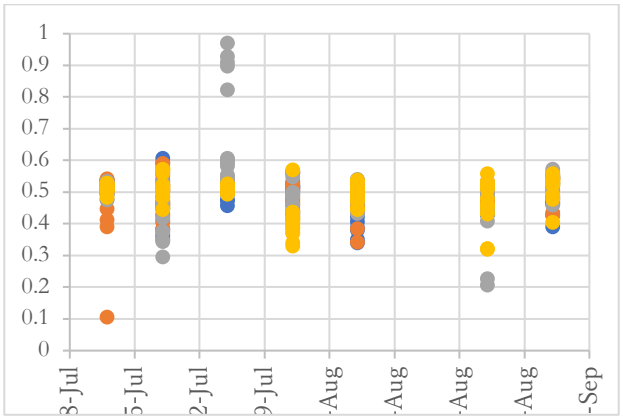

Fig. 2: N_2O concentration of all treatments during the study

Based on the results of data processing, the Macropore treatment produced the tallest plants, followed by the MFC treatment. However, field observations revealed that treatments involving MFC (MFC or MFC+MP) resulted in the tallest plant growth.

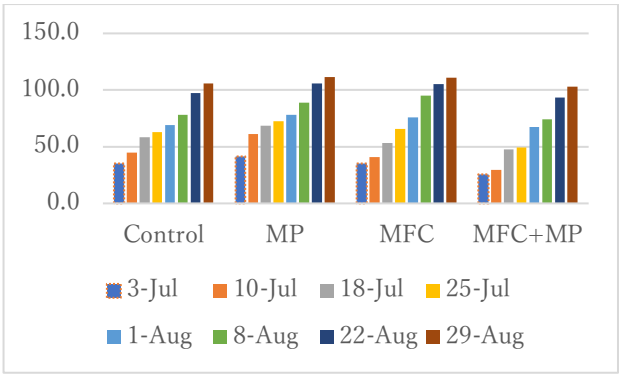

Fig. 3: Plant height during research

ACKNOWLEDGMENTS

I would like to express my sincere gratitude to the MEXT scholarship for providing me with the opportunity to conduct this research.

REFERENCES

Davis JB and Yarbrough HF (1962) Preliminary Experiments on a Microbial Fuel Cell Two in Its Metabolism , Might Produce Measurable Current. Such Was the Case. When Escherichia Coli Was Added to the Biological Half-Cell with Glucose as Substrate, The Open Circuit Voltage in- Creased Fr. Virology: 1–2.

Insam H and B Wett (2008) Control of GHG emission at the microbial community level. Waste Management 28(4): 699–706. doi: 10.1016/j.wasman.2007.09.036.

Predicting Rice Yields with Deep Learning Using UAV-Based Multispectral Imagery and Weather Data

Md. Suruj Mia[1], Ryoya Tanabe[2], Luthfan Nur Habibi[1], Naoyuki Hashimoto[3], Koki Homma[4], Masayasu Maki[5], Tsutomu Matsui[6] and Takashi S. T. Tanaka[6,7]

[1] The United Graduate School of Agricultural Science, Gifu University, Gifu 501-1193, Japan
[2] Graduate School of Natural Science and Technology, Gifu University, Gifu 501-1193, Japan
[3] Faculty of Agriculture and Marine Science, Kochi University, Kochi 783-8502, Japan
[4] Graduate School of Agricultural Science, Tohoku University, Miyagi 980-8572, Japan
[5] Faculty of Food and Agricultural Sciences, Fukushima University, Fukushima 960-1296, Japan
[6] Faculty of Biological Sciences, Gifu University, Gifu 501-1193, Japan
[7] Artificial Intelligence Advanced Research Center, Gifu University, Gifu 501-1193, Japan

INTRODUCTION

Yield monitoring and satellite-based remote sensing technologies have been developed to measure the spatial distribution of crop yields in large-scale farming practices. In agriculture, timely, nondestructive, inexpensive, and reliable large-scale yield forecasts are important and prerequisite for preventing climate risks and ensuring food security (Wang et al. 2014). Precision agriculture involves collecting, processing, and analyzing temporal and spatial data and integrating it with other relevant information to support resource-efficient management decisions. However, the precision of yield predictions has often been constrained by the limited spatial and temporal resolution of satellite data (Wang et al. 2010). In response to these challenges, unmanned aerial vehicles (UAVs) have been widely used to collect data due to their superior spatial, spectral, and temporal resolutions compared to airborne and satellite plat-forms (Maimaitijiang et al. 2020).

Yield estimation models are very dependent on substantial and specific input information and require huge computational costs (Cai et al. 2019). Machine learning algorithms possess the capability to devise novel solutions for real-world challenges, enabling farmers to make informed decisions while requiring minimal or even no human intervention (Srivastava et al. 2022). Among all machine learning techniques, Convolutional Neural Network (CNN) algorithm is efficient in image classification and analysis and able to predict crop yield accurately (Fu et al. 2022, Tanabe et al. 2023 and Yang et al. 2019). Weather is one of the major environmental factors affecting crop growth and yield. Incorporating weather data after image acquisitions into CNN models may enhance the precision of the yield prediction model. CNN models are recognized for their demanding computational needs and substantial memory requirements, which can limit their applicability in resource-constrained environments. It is widely acknowledged that enhancing CNN architectures by increasing depth and width can lead to improved model performance (Alzubaidi et al. 2021). However, increasing the depth of the architecture after the integration of weather and image data may also contribute to improving yield prediction accuracy.

The objective of this study was to develop a multimodal deep learning model to predict rice grain yield using UAV images at the heading stage and weather data.

MATERIALS AND METHODS

Rice yield surveys were conducted in 22 farmers' fields in Japan over six years (2017–2022). Nine rice varieties were planted, and crop management was conducted according to local conventional methods. Strip trials were performed in 12 fields for basal fertilizer application to obtain high yield variability and to determine whether the effect of fertilizer application rate on rice yield could be evaluated using a predicted yield map. A total of 894 samples were collected in all yield surveys, from an area of approximately 1.0 m^2 at the heading stage. UAV multispectral images and weather data (https://amu.rd.naro.go.jp) for each region were collected and processed. 18 architecture models consisting of two types of CNN feature extractor layers (i.e., CNN_2conv and AlexNet), three different depths of fully connected layers, and three methods of integrating weather data (no weather data, weekly sum of weather data, and monthly sum of weather data) into deep neural network models were established. The model's performance was assessed by employing the R^2, root mean squared error (RMSE), and root mean squared percentage error (RMSPE) metrics. The statistical analysis was conducted using Python (version 3.8.10) and SciPy (version 1.9.1). An analysis of variance (ANOVA) was executed to assess how the architectures influenced the model's performance. Tukey's honestly significant difference test (Tukey's HSD) was employed to detect disparities in the mean performance values of the models. In all the analyses, a significance level of $p < 0.05$ was adopted.

RESULTS

The distribution of collected data was approximately normal. The mean value was 6.65 t ha^{-1}, and the standard deviation was 1.46 t ha^{-1}. There was no significant difference between the AlexNet and CNN_2conv

architectures. The effects of the number of layers and weather data types on the model performance were significant but according to Tukey's HSD results, there were no significant differences among various layers. The top two accurate models with the lowest RMSE values were found in models integrating weekly weather data as input data with either AlexNet or CNN_2conv (Table 1). Using the optimal models from both architectures, the yield maps predicted (one On-Farm Experimentation field) are illustrated in Fig. 1. These yield maps, for both scenarios, reveal variations in yield across the field, with distinct areas where various rates of basal fertilizer were applied.

Table 1: Performance of best CNN models of both architecture for predicting rice yields

	Alexnet architecture		CNN architecture	
	Train	Test	Train	Test
R^2	0.66	0.65	0.68	0.65
RMSE (tha^{-1})	0.842	0.859	0.821	0.860
RMSPE (%)	14	14	13	14

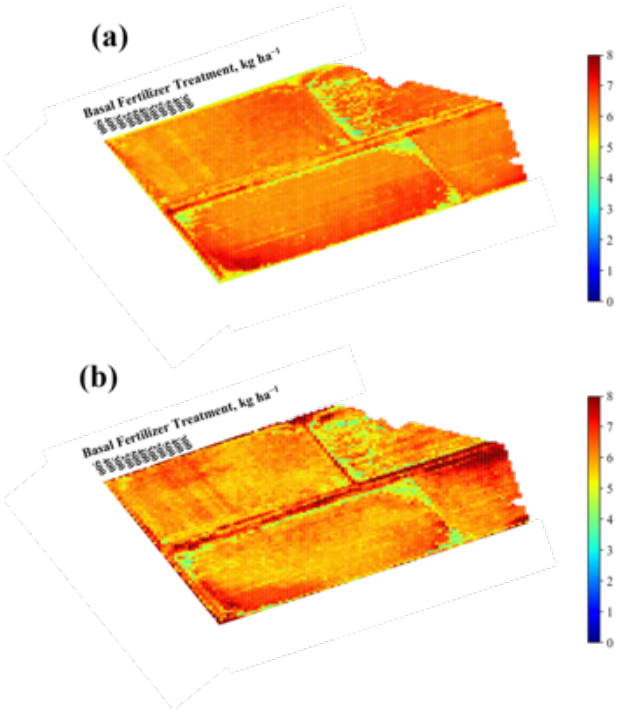

Fig. 1: Yield prediction map by using (a) Alexnet architecture-based CNN model and (b) CNN_2conv architecture-based CNN model.

DISCUSSION

This research investigates the capability of multimodal deep learning models, utilizing UAV multispectral and weather data, to achieve highly accurate predictions of rice yield. Models trained with weekly weather data consistently outperform others. There has the spatial variation of predicted yield maps across the different models, despite similar prediction accuracy. By incorporating weekly weather data and simplifying the CNN architecture, farmers and researchers can make more accurate predictions, optimize resource allocation, and improve overall agricultural sustainability.

REFERENCES

Alzubaidi L, Zhang J, Humaidi AJ, Al-Dujaili A, Duan Y, Al-Shamma O et al. (2021) Review of deep learning: Concepts, CNN architectures, challenges, applications, future directions. J. Big Data, 8: 53.

Cai Y, Guan K, Lobell D, Potgieter AB, Wang S, Peng J et al. (2019) Integrating satellite and climate data to predict wheat yield in Australia using machine learning approaches. Agric. Meteorology, 274: 144–159.

Fu Z, Yu S, Zhang J, Xi H, Gao Y, Lu R et al. (2022) Combining UAV multispectral imagery and ecological factors to estimate leaf nitrogen and grain protein content of wheat. Eur. J. Agron., 132: 126405.

Maimaitijiang M, Sagan V, Sidike P, Hartling S, Esposito F and Fritschi FB (2020) Soybean yield prediction from UAV using multimodal data fusion and deep learning. Remote Sens. Environ., 237: 111599.

Srivastava AK, Safaei N, Khaki S, Lopez G, Zeng W, Ewert F et al. (2022) Winter wheat yield prediction using convolutional neural networks from environmental and phenological data. Sci. Rep., 12: 3215.

Tanabe R, Matsui T and Tanaka TST (2023) Winter wheat yield prediction using convolutional neural networks and UAV-based multispectral imagery. Field Crops Res., 291: 108786.

Wang K, Franklin SE, Guo X and Cattet M (2010) Remote sensing of ecology, biodiversity and conservation: A review from the perspective of remote sensing specialists. Sensors, 10: 9647–9667.

Wang L, Tian Y, Yao X, Zhu Y and Cao W (2014) Predicting grain yield and protein content in wheat by fusing multi-sensor and multi-temporal remote-sensing images. Field Crops Res., 164: 178–188.

Yang Q, Shi L, Han J, Zha Y and Zhu P (2019) Deep convolutional neural networks for rice grain yield estimation at the ripening stage using UAV-based remotely sensed images. Field Crops Res., 235: 142–153.

Biological Weed Control Through Weed Predation by Pill Bugs (*Armadillidium vulgare* L.) in Nursery of Tea Tree (*Camellia sinensis*)

Niken Nabilaputri Pranaasri[1, 2] and Yamashita Masayuki[2]

[1] The United Graduate School of Agriculture Science, Gifu University, 1-1 Yanagido, Gifu-shi, Gifu 501-1193, Japan
[2] Graduate School of Integrated Science and Technology, Shizuoka University, 836 Ohya, Suruga, Shizuoka 422-8529, Japan

INTRODUCTION

Tea is one of the world's most valuable commodities. To achieve high production, optimal cultivation is critical. Weeds are one of the main challenges limiting productivity in the fields. According to Peiris and Nissanka (2016), uncontrolled broadleaf weeds can cover 15% of the ground area of a tea plantation. Weeds that grow rapidly harm the tea plants, causing poor bush frame. Weeds that grow on the edges of the tea fields obstruct tea plantation management and serve as hosts for pests (Ichihara et al, 2020).

For decades, herbicides have been widely used to control weeds. However, excessive use of herbicides has led to herbicide-resistant weeds. In Japan, glyphosate-resistant grass weeds *Lolium multiflorum* (Italian ryegrass) and *Eleusine indica* (Indian goosegrass) were detected in rice paddy levees in 2011 (Heap, 2023). In terms of ecology, the use of herbicide leaves chemical residue in the ecosystem. Therefore, another effective weed control method is necessary. Instead of using chemicals, biological weed control takes advantage of the benefits from ecosystem. Seed-predators are one of the beneficial organisms. Ichihara et al (2012) reported that seed predation by ground insects effectively decreases seed emergence of Italian ryegrass.

Pill bugs (*Armadillidium vulgare* L.) are terrestrial isopods that are common in grassland (Souty-Grosset and Faberi, 2018), and they feed on both dead and living plants. Saska (2008) discovered that pill bugs are observed feeding on plant seeds. According to our prior study, pill bugs were identified in abundance in tea fields. Therefore, the potential roles of pill bugs as weed control in tea fields are necessary to be investigated. Furthermore, since the presence of weeds might interfere with the tea plants, the relationship between the presence of pill bugs, weeds, and tea plants is also essential to be explored. The main aim of this study is to examine the potential role of weed predation by pill bugs as a biological weed control in the nursery of tea plants.

MATERIALS AND METHODS

The experiment was carried out in the experiment field of Shizuoka University from July 4th to August 22th, 2023. Before the experiment, pill bugs were collected on the campus of Shizuoka University and kept in incubators in the laboratory at 25°C 12:12 LD.

Soil was filled up to 80% of containers sized 72 cm x 26 cm x 40 cm. Two 12-months-old tea trees were planted in the middle of the containers (±15 cm apart) for each container. There were four treatments, each with 3 replicates: (A) tea tree only, (B) tea tree + weed seeds, (C) tea tree + pill bugs, and (D) tea tree + weed seeds + pill bugs. For the treatment using weed seeds, five weed species were used, *Crassocephalum crepidoides* (Redflower ragleaf), *Eleusine indica* (Indian goosegrass), *Lolium multiflorum* (Italian ryegrass), and *Taraxacum sp* (Dandelion), with seed sizes 2 mm, 4 mm, 6 mm, and 4 mm, respectively. Fifty seeds of each weed species were distributed at random to the containers of treatment B and D. For the treatment using pill bugs, 30 male pill bugs with a length of approximately 2 cm were added to the containers of treatment C and D. Five individuals of pill bugs were added every week. To keep other insects and birds out, the containers were netted. Water sprinklers were installed for daily watering.

To investigate the effects of pill bugs on weeds, the germination rates were calculated by counting the number of germinated seeds in treatments B and D every week. To examine the effects of pill bugs and weeds on the tea tree growth, leaves number of the tea tree was recorded in the all treatments.

RESULTS

The germination rates of weeds were recorded to be significantly lower on *C.crepidoides*, *Taraxacum* sp., and *L.multiflorum* with pill bugs (in treatment B) compared to those without pill bugs (in treatment D). In contrast, the germination rates in *E.indica* did not differ between the two treatments. However, there is a trend that its germination rates tended to be lower in the treatment B (Fig.1). Pill bugs were observed feeding on the weed seeds and seedlings. The seedling predation rates of each weed species on *C.crepiroides*, *Taraxacum* sp., *L.multiflorum*, and *E,indica* were from 12.5% to 29.3%. These results suggested that seedling predation by pill bugs was varied among the weed species.

In the observation on tea tree, the results showed that the leaf numbers of the tea did not differ among treatments, yet it can be seen that a trend showed the leaf numbers in the treatment D was slightly higher compared to the other treatments (Fig.2).

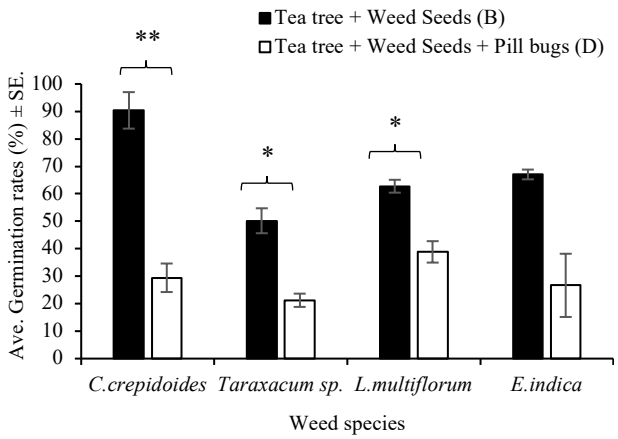

Fig.1. Germination rates of four weeds species in treatment without pill bugs (B) and with pill bugs (D).

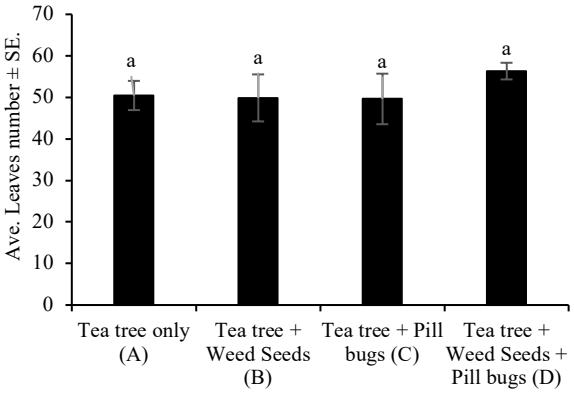

Fig.2. Average of leaves number of tea tree in each treatment.

DISCUSSION

This study revealed that pill bugs are effective in decreasing the weed population by reducing the number of germinated seeds. Further, this study suggested that the decrease in seed emergence was caused by seed predation. Pill bugs feed on the seeds of the weeds regardless of the weed species. However, during the predation activity, pill bugs have different seed preferences depending on the weed species. Seeds of *C.crepidoides* are preferable to *Taraxacum* sp. and *L.multiflorum*. Saska (2008) stated that the size of weed seeds influences predator attack encounters in post-dispersal seed predation. In this study, *C.crepidoides* was the smallest-sized seed and *L.multiflorum* was the largest-sized seed among the used weed species.

Pill bugs have been observed feeding on weed seeds and seedlings, implying that they play roles in weed control. Seed banks have been demonstrated to have a significant impact on weed growth and population dynamics. The presence of pill bugs may aid in reducing the seed bank through weed seed predation. Furthermore, seedling predation by pill bugs will cause damage and hamper the weed development. The results of this study then suggested that weed predation by pill bugs may be used as biological weed control in the future.

When pill bugs are present, the weed population can be suppressed. This will decrease the competition between tea trees and weeds, allowing the tea to grow better. Meanwhile, when pill bugs are not present, the weed populations are not controlled. Massive growth of weeds will interfere with the tea trees and may alter the growth of tea trees. Tea nursery (8-18 months old after planting) is said to be the critical period for weed intervention (Deka and Barua, 2015). The development of the tea bushes in tea nursery may be blocked by the growth of the weeds.

The presence of pill bugs was not adversely affecting the growth of the tea tree, especially when weeds were present together with the tea tree. Pill bugs are soil-surface organisms. In this situation, dispersal seeds are easier to reach, hence, they tend to graze on the weeds rather than the tea trees (Fig.2). In addition, since tea trees are woody plants, they are considerably hard to be ingested by pill bugs. This may create the pill bug's predilection for weeds and tea trees.

REFERENCES

Deka J and Barua I C (2015) Weed of tea fields and their control. National Seminar on Plant Protection in Tea. Tea research Association Tocklai Tea Research Institute Jorhat, Assam, India.

Heap I (2023) The International Herbicide-Resistant Weed Database Online. www.weedscience.org (Accessed on 12 October 2023)

Ichihara M, Inagaki H, Matsuno K, Saiki C, Yamashita M, and Sawada H (2012). Postdispersal seed predation by *Teleogryllus emma* (Orthoptera: Gryllidae) reduces the seedling emergence of a non-native grass weed, Italian ryegrass (*Lolium multiflorum*). Journal of Weed Biology and Management, 12: 131–135.

Ichihara M, Togawa M, and Haga H (2020) Vegetation in tea field margins and climbing plants on tea bush canopies in Shizuoka Prefecture, Japan. J. Weed. Sci. Tech., 65: 114–117. (In Japanese)

Peiris H M P and Nissanka S P (2016) Affectivity of chemical weed control in commercial tea plantations: A case of study in Hapugastenne Estate, Maskeliya, Sri Lanka. Procedia Food Science, 6: 318–322.

Saska P (2008) Granivory in terrestrial isopods. Ecological Entolomogy, 33: 742–747.

Souty-Grosset C and Faberi A (2018) Effect of agricultural practices on terrestrial isopods: A review. Zookeys, 801: 63–96.

FEM Analysis of Withdrawal Performance of Self-Tapping Screw and Cross-Laminated Timber Joint

Sarah Amira[1,2], Kenji Kobayashi[2] and Keita Ogawa[2]

[1] The United Graduate School of Agricultural Science, Gifu University, 1-1 Yanagido, Gifu 501-1193, Japan
[2] Faculty of Agriculture, Shizuoka University, 836 Ohya, Suruga-ku, Shizuoka 422-8529, Japan

INTRODUCTION

Cross-laminated timber (CLT) is an engineered wood product used in wooden houses to achieve environmental sustainability in Europe, Australia, and North America. Interest in CLT as a newly developed technology has increased in Japan. Izzi, et al. (2018) stated that CLT structures exhibit satisfactory performance under seismic conditions because of the high strength-to-weight ratio and in-plane stiffness of the CLT panels and the capacity of connections to resist loads with ductile deformations and limited strength impairment.

Self-tapping screw (STS) optimized primarily for axial loading, represent the state-of-the-art fastening and reinforcement technology in CLT construction (Mohammad et al., 2013; Kobayashi, 2015; Dietsch and Brandner, 2015). Recently, the Japanese Industrial Standard for STSs for timber joints (JIS A 1503) has been published. However, this standard does not include withdrawal strength and head pull-through properties because their inclusion requires the consideration of the properties of the adjacent wood; the JIS is primarily focused on the fastener property (Goto et al., 2018).

The appropriate modelling and formulations in finite element method (FEM) simulation can be a non-destructive analysis for the precaution of the possible withdrawal deformations occurrence of the CLT-STS joint resisting the withdrawal load on STS, which is difficult to be visually observed in the laboratory experiment. Previous studies have numerically and theoretically investigated the mechanism of axially loaded STS withdrawal strength through the wooden member with the simplified models (Avez, et al., 2016; Honda et al., 2021). Through the linear elastic analysis from FEM, the simulation results generally follow the stiffness trend of the experimental values. However, the failure modes and deformation were less representative due to the simplified models. This study evaluated the initial stiffness of an STS inserted into small pieces of CLT where the 3D models were made more precise and as similar as possible to the actual shape, concerned with the orientation of each lamina in CLT layers in the same state of the specimen as the experimental withdrawal test, and the deformations that occurred within both components were observed through FEM simulation.

MATERIALS AND METHODS

Materials—The withdrawal strength of a single STS inserted into a CLT was measured using a withdrawal loaded test. The test materials used in this study were composed of small pieces of five-layered CLT made of sugi (*Cryptomeria japonica* D. Don) lamina. Two types of connectors, fully threaded STS (PX8-260) and partially threaded STS (PS8-260), manufactured by Synegic Co., Ltd., with a thread diameter of 8 mm and total length L of 260 mm were considered and distinguished by the effective length of the STS threaded part inserted into the specimen l_{ef} (mm) (the shapes of the screw head and screw tip were ignored). The l_{ef} of the fully threaded STS varies depends on the thickness of the CLTs, whereas those of the partially threaded STSs were set to 80 mm.

Withdrawal test—The STS was driven through the entire test specimen in order to avoid the tip influencing the layer orientation, as shown in Fig 1. A turned washer with a diameter of 8 mm was used to fix the screw head to the screw grip. A screw grip shaped to fit the head of the STS was attached to the load head of a universal testing machine (UTM, Shimadzu Co., AG-I 250 kN) for applying the monotonic static load at a constant rate of 1 mm/min. Four displacement gauges, one pair of CDP-10 with a capacity of 10 mm and one pair of CDP-25 with a capacity of 25 mm (manufactured by Tokyo Measuring Instruments Laboratory Co., Ltd.), were attached in the crossway each other to record the displacement during the withdrawal test.

FEM simulation—The 3D models consisted of the STS inserted into CLT were created using Autodesk Fusion 360 software and imported to the MSC Marc/Mentat commercial finite element software as solid body and generated a mesh that consisted of linear tetrahedral volumetric elements (with hybrid elements for partially threaded STS). Ten solid mesh seeds were applied to the edge of the thread-profiled hole on CLT as a parameter of the generated mesh elements number around the STS-adjacent CLT. The mesh element of CLT was splined in order to gives a more accurate representation of the actual physical geometry and a more accurate calculation of the normal vector (HEXAGON, 2022). Elements of the CLT body were defined as elastic-plastic orthotropic material, while elements of the STS body were defined as an elastic-plastic isotropic material. Therefore, the longitudinal grain orientations were projected in x axis for the odd layers (layers 1, 3, and 5) and y axis for the even layers (layers 2 and 4). The material properties of sugi wood according to wood industry handbook (Forestry and Forest Products Research Institute, 2004) and steel was modelled as an elastic and perfectly plastic material and the Hill criterion was used for wood. The loads subjected

to the specimen were approximated to the mesh elements in boundary condition. The withdrawal displacement was defined as fixed displacement applied to the six nodes on the screw head surface in positive *z*-axis direction, while the CLT elements were fixed to zero in the axial and rotational to the *z*-axis with the slight fixed *x* and *y*-axes to keep the main position.

RESULTS AND DISCUSSION

Comparison between FEM simulation and experimental results—In the current progress, the FEM simulation prescription were only attaining the elastic to plastic state after 111 trials. The softening behaviour after a maximum load has been reached could not be represented from the simulation due to damaged softening behaviour can lead to numerical solution non-convergence (Zhang, Chun, Lin, Wang, & Li, 2022). Therefore, the initial stage of the scheme of axial static loading subjected to a STS inserted into CLT was evaluated in linear elastic analysis by comparing the initial stiffness $K_{0.1\sim0.4}$ (the stiffness within the range of 10-40% of maximum load). The initial stiffness obtained from FEM simulation overestimated those of experimental result 22% for CLT with fully threaded STS and 38% for partially threaded STS, as projected in Fig. 1. As the prescriptions of the FEM simulation described the CLT as an orthotropic material, the other natural characteristics of wood have not well represented yet and it was leading to the uncompleted static load and displacement curve as intended.

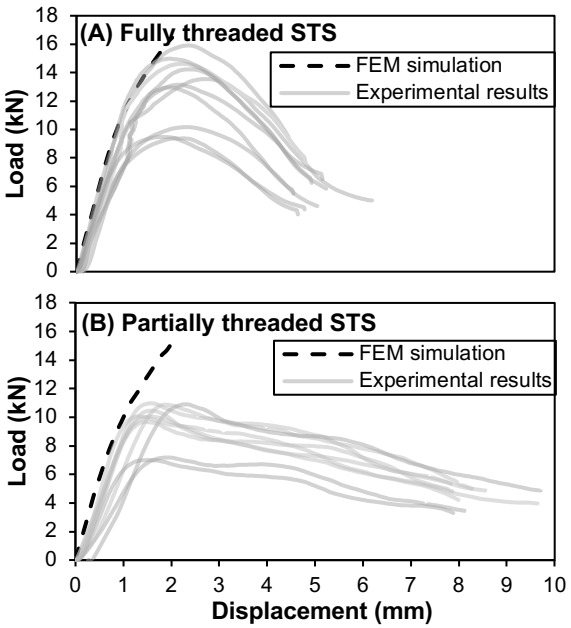

Fig. 1: Load-displacement comparison of FEM simulation and experimental result. (A) CLT with fully threaded self-tapping screw; (B) CLT with partially threaded self-tapping screw.

Visualisations of withdrawal deformations—The deformation observed visually through the contour bands scalar simulation results. Withdrawal failure is an initial failure in withdrawal test, characterized by the shear failure at the wooden members surrounding the STS to the sticking out of the upmost layer of CLT around the STS (Pang et al., 2020). Within two seconds of simulation, the major displacement of the CLT member with fully threaded STS occurred along the STS threads-contacted parts with the highest withdrawal displacement at 1.599 mm and the surface of the upmost layer was sticking out which is also found on the experimental withdrawal failure. In the model of those with partially threaded STS, withdrawal deformation occurred inside the CLT member that only in contact with the threads section of partially threaded STS with the maximum displacement of 4.008 mm.

REFERENCES

Avez C, Descamps T, Serrano E and Le´oskool L (2016) Finite element modelling of inclined screwed timber to timber connections with a large gap between the elements. Eur. J. Wood Prod., 74: 467–471.

Dietsch P and Brandner R (2015) Self-tapping screws and threaded rods as reinforcement for structural timber elements - a state-of-the-art report. Construction and Building Materials, 97: 78–89.

Forestry and Forest Products Research Institute. (2004). Wood Industry Handbook 4th Revised Edition], pp. 135–136. Maruzen Publishing. Tokyo. (In Japanese)

Goto Y, Jockwer R, Kobayashi K, Karube Y and Fukuyama H (2018) Legislative background and building culture for the design of timber structures in Europe and Japan. World Conference on Timber Engineering. Seoul, Republic of Korea.

HEXAGON. (2022). Marc Volume A: Theory and User Information. Hexagon. California, United States.

Honda W, Ochiai Y, Aoki, K and Inayama M (2021) Mechanism of Withdrawal Resistance of Screws Embedded Perpendicular to Grain and Evaluation Method of Withdrawal Strength. Mokuzai Gakkaishi, 67(4): 178–187. (In Japanese with English abstract)

Izzi M, Casagrande D, Bezzi S, Pasca D, Follesa M and Tomasi R (2018) Seismic behaviour of Cross-Laminated Timber structures: A state-of-the-art review. Engineering Structures, 170: 42–52.

Kobayashi K (2015) Present and future tasks for screw joints in timber structures. *Mokuzai Gakkaishi*, 61(3): 162–168. (In Japanese with English abstract)

Mohammad M, Douglas B, Rammer D and Pryor SE (2013) Chapter 5 - Connections in cross-laminated timber buildings. In: E. Karacabeyli, and B. Douglas (Eds.), CLT handbook: cross-laminated timber, pp. 3–44. FPInnovations. Canada.

Pang SJ, Ahn KS, Kang SG and Oh JK (2020) Prediction of withdrawal resistance for a screw in hybrid cross-laminated timber. J. Wood Sci., 66(79): 1–11.

Zhang C, Chun Q, Lin Y, Wang H and Li P (2022) Experimental and nonlinear finite element. J. Wood Sci., 68(41): 1–18.

Effects of Ultraviolet Light on the Post-harvest Quality of Cherry Fruits (*Prunus avium* L.)

Nabila Nurul Ahmeidiati, Teppei Imaizumi, Manasikan Thammawong and Kohei Nakano

The United Graduate School of Agriculture Science, Gifu University, 1-1 Yanagido, Gifu-shi, Gifu 501-1193, Japan

INTRODUCTION

Cherries are considered a remarkable nutritious fruit that contains substantial quantities of vital nutrients and bioactive elements. These include glucose, fructose, vitamin C, anthocyanins, quercetin, flavan-3-ols, flavonols, and hydroxycinnamates (Zhang et al., 2021). The decline in quality observed in cherry fruits from the time of harvest to consumption can be attributed to various factors, including physical alterations, chemical transformations, enzymatic reactions, and microbiological changes. The potential repercussions of this quality degradation resulting from microbial activity pose a significant threat to consumers, as it may lead to the presence of harmful toxins or pathogens. Additionally, it is accompanied by economic losses stemming from these deteriorations (Saparov et al., 2023). Therefore, the preservation of cherry fruits over an extended period is significantly important, serving the dual purpose of facilitating fruit marketing and preserving its quality attributes. The degradation of vitamin C during processing and storage is a significant concern for nutrition experts, food processors, and consumers alike. Vitamin C is employed as a gauge of the health-related quality of fruits because it is more susceptible to deterioration when compared to other beneficial compounds.

Ultraviolet (UV) radiation is considered to be germicidal against microorganisms such as bacteria, viruses, protozoa, yeasts, moulds and algae (Keyser et al., 2008). It disrupts the cellular DNA of a wide range of microorganisms by changing the formation of pyrimidine dimers, and it has been frequently employed for disinfection purposes (Bintsis et al., 2000). However, it must be noted that overexposure of UV light may result in lipid peroxidation, membrane damage as well as programmed cell death and thus shorten the shelf life of fresh produce if not in the correct dosage. Therefore, the most efficient dosage of UV light radiation to preserve the quality of cherry fruits is investigated. Especially in vitamin C as one of the main nutrients in cherry fruits.

MATERIALS AND METHODS

A fresh cherries from Yamagata Prefecture subjected to various dosage of UV-C radiation of 0 mJ/cm^2 , 50 mJ/cm^2 , 100 mJ/cm^2, 150 mJ/cm^2, and 1000 mJ/cm^2 was transported to lab in Gifu Universty, Gifu Prefecture by commercial delivery company. Duration of the transporation was around 2 days. Cherries then stored for 14 days under the temperature of 0.5 °C in incubator.

Vitamin C

A pitted fresh cherry around 4 grams (+/- 1 gram) was finely chopped and extracted with 15 mL of metaphosphoric acid. The homogenized solution of cherry is measured using High Performance Liquid Chromatography (HPLC). The amount of vitamin C per 100 grams of cherries was calculated. Vitamin C was measured in day 0, day 2, day 4, day 6, day 8, day 10, day, 12, and day 14.

RESULTS

On Day 0 of the storage, as seen on Fig.1, vitamin C levels exhibited higher concentrations for cherries subjected to UV exposures of 0 mJ/cm^2, 50 mJ/cm^2, and 1000 mJ/cm^2, while lower concentrations were observed for those exposed to UV 100 mJ/cm2 and 150 mJ/cm^2.

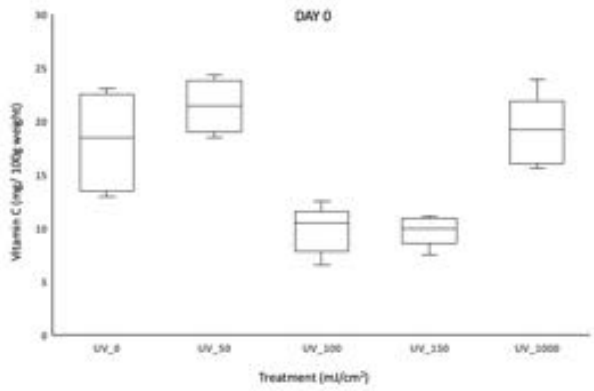

Fig. 1 : Vitamin C of cherry fruits during Day 0 storage.

This concentration of vitamin c collerates with color of the fruits (Fig 2), where it is shown in the visual observation that cherries exposed with UV 100 mJ/cm^2 and 150 mJ/cm^2 has lighter color compared to the one with higher vitamin C concentration.

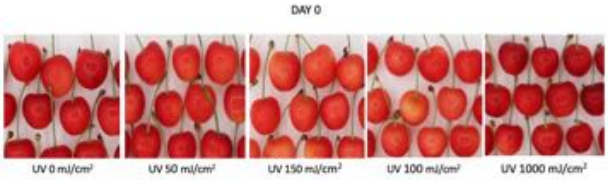

Fig. 2: Cherry fruits color observed in Day 0 storage.

Observed until the day 14 of storage (Fig.3), a gradual decline in vitamin C levels was noted over time for cherries exposed to UV 0 mJ/cm^2, 50 mJ/cm^2, and 1000 mJ/cm^2, with minimal fluctuations in the vitamin C levels for those exposed to UV 100 mJ/cm^2 and 150 mJ/cm^2. It is hypothesized that cherries exposed to UV levels of 0, 50 mJ/cm^2, and 1000 mJ/cm^2 experienced a gradual reduction in vitamin C content from Day 0 to Day 14. In contrast, cherries subjected to UV 100 mJ/cm^2 and 150 mJ/cm^2 exhibited a swift decline in vitamin C content within a single day, likely attributable to the stress induced by UV radiation.

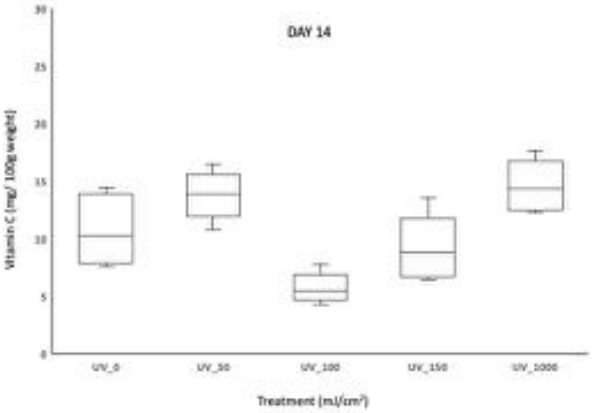

Fig. 3: Vitamin C of cherry fruits during Day 14 storage

DISCUSSION

The initial divergence in vitamin C concentrations on Day 0, with higher levels in cherries exposed to 0 mJ/cm², 50 mJ/cm², and 1000 mJ/cm² of UV, compared to lower levels in those exposed to 100 mJ/cm² and 150 mJ/cm², suggests a differential response to UV radiation. This initial contrast may be attributed to the induction of protective mechanisms in cherries exposed to lower UV levels, potentially triggering the synthesis defense compounds that disturb the production of vitamin C as can be seen to effect the vitamin C level of 100 mJ/cm² and 150 mJ/cm² exposure. However, once it reaches saturation, the defense mechanism get deactivated and vitamin C is produced without disruption, as observed in 1000 mJ/cm² of UV exposure which is way higher than its counterpart.

The gradual reduction in vitamin C levels observed over the course of the study for cherries exposed to UV 0 mJ/cm², 50 mJ/cm², and 1000 mJ/cm² indicates a sustained oxidative stress response. It is plausible that these cherries were able to maintain a certain degree of defense against UV-induced oxidative damage, slowing the degradation of vitamin C over time. This could be due to the activation of antioxidant systems or the presence of protective compounds that counteracted the effects of UV exposure. As seen on Fig. 2, UV 0 mJ/cm², and 50 mJ/cm² treated cherry that are more pale compared to other treatment, it may indicates that UV 0 mJ/cm², and 50 mJ/cm² delay the production of anthocyanin which is the main pigment in red colored fruits. Gao and Maza (1999) mentioned that the color of cherries is predominantly determined by the arrangement and amount of various anthocyanins present in their skin.

In contrast, cherries exposed to UV 100 mJ/cm² and 150 mJ/cm² exhibited a swift decline in vitamin C content within a single day. This rapid reduction can be attributed to the higher levels of UV radiation, which overwhelmed the cherries' antioxidative capacity. Such exposure might have led to the increased production of reactive oxygen species, leading to a faster degradation of vitamin C. It is essential to consider that high levels of UV radiation may not only trigger oxidative stress but could also directly affect the stability of vitamin C.

Overall, the findings suggest that cherries have a differential response to UV exposure, with low levels of UV potentially stimulating protective mechanisms, while high UV levels lead to rapid vitamin C degradation until it reaches certain saturation where vitamin C level increases again. Further research is needed to explore the specific biochemical and molecular mechanisms underlying these responses. Understanding these mechanisms can have significant implications for optimizing cherry preservation and enhancing their nutritional value under various environmental conditions.

REFERENCES

Bintsis T, Litopoulou-Tzanetaki E and Robinson RK (2000). Existing and potential applications of ultraviolet light in the food industry–a critical review. Journal of the Science of Food and Agriculture, 80(6): 637–645.

Gao L and Mazza G (1995) Characterization, quantitation, and distribution of anthocyanins and colorless phenolics in sweet cherries. Journal of Agricultural and Food Chemistry, 43(2): 343–346.

Keyser M, Műller IA, Cilliers FP, Nel W and Gouws PA (2008) Ultraviolet radiation as a non-thermal treatment for the inactivation of microorganisms in fruit juice. Innovative food science and emerging technologies, 9(3): 348–354.

Saparov DE, Sultonova SA, Pulatov MM and Boltaboyev KK (2023) Experimental study of processing sweet cherries with ultraviolet radiation. In IOP Conference Series: Earth and Environmental Science, 1231(1): p.012033.

Zhang Q, Yang W, Liu J, Liu H et al. (2021). Postharvest UV-C irradiation increased the flavonoids and anthocyanins accumulation, phenylpropanoid pathway gene expression, and antioxidant activity in sweet cherries (*Prunus avium* L.). Postharvest Biology and Technology, 175: 111490.

Quantitative Analysis of Japanese Commercial Coating Penetration into *Fagus crenata* Blume Wood Using X-ray Microtomography

Tyana Solichah Ekaputri[1], Ayuni Nur Apsari[1], Takashi Tanaka[2] and Kenji Kobayashi[2]

[1] The United Graduate School of Agricultural Science, Gifu University, 1-1 Yanagido, Gifu-shi, Gifu 501-1193, Japan
[2] Graduate School of Integrated Science and Technology, Shizuoka University, Oya 836, Suruga-ku, Shizuoka City 422-8529 Japan

INTRODUCTION

The use of film thin layer has become ubiquitous practice across much of the scientific and industrial sector, recently. Coatings can enhance physical, chemical and aesthetic properties with lower the costs of the final product. Coating applications such as varnish, stain and paint, are commonly used in the furniture industry.

The interactions between coatings and natural material like wood and the very complex formulations of coatings make predictions of their service life and performance challenging (Hazir and Koc, 2021). Coatings are used to obtain a synergistic action between the characteristics of substrate and the covering materials (Hazir and Koc, 2019). The fact well-known that the coating performance namely adhesion is depending on a hygroscopic characteristic of wood composite panels (Dilik, et al., 2014). Therefore, coating type plays an important role on coating performance such as film thickness which affects the abrasion resistance and the adhesion of the coating itself. According to Cassens and Feist (1986), finishing characteristics of coatings on wood surfaces depend on a large number of variables, of which the coating-film thickness is an important one. In addition, the penetration of the coating into the wood become important for several reasons. Firstly, coating penetration can improve water repellence and dimensional stability and reduce the surface cracks. Second, the adhesion of the coating to the wood material will benefit from a certain degree of penetration as well such as mechanical entanglement or interlocking, adsorption interaction by polar and dispersive forces, and intermolecular diffusion. Third, coating contained fungicides might have improved penetration of the fungicide because it penetrates together (Meijer, 1998).

Coating penetration is mainly determined by the ability of the coating to flow into the lumina of either tracheid or ray-cells. Therefore, the anatomical microscopic penetration is fundamental to be investigated. In previous study by Ekaputri et al. (2021), Japanese commercial coatings penetration into Fagus crenata veneer was successfully visualized using X-ray microtomography that resulted in 2D and 3D images. To deeply understand the penetration scheme of coating materials into wood affected by the chemical content of it, the quantitative analysis is important to be investigated.

Accordingly, the aim of this study was to determine the effects of chemicals on the coating penetration using X-ray microtomography for coatings applied to the surface of Japanese beech (Fagus crenata Blume).

MATERIALS AND METHODS

Fagus crenata Blume veneer was prepared with dimension 300 mm x 300 mm x 1.3 mm. Four veneers were prepared and proceed with cold-pressing and hot-pressing with the pressure 1 MPa for 20 min and hot-pressed with pressure 1 MPa at 125 °C for 4 min. After cooling down, the veneers were cut into 100 mm x 100 mm (length and width) for the coated veneer and one control sample.

Japanese commercially available coating was purchased from Shizuoka, Japan. The specification of coating used to finish the veneer sample explained on Table 1.

Table 1. Coating specifications

Material Name	Color	Ingredients That Might Affect X-ray Interaction	Percentage (%)	Chemical Formula
Aspen Lacquer Spray (Asahipen)	Brown (BR)	Titanium Dioxide	0.1–1	TiO_2
	Matte White (MW)	Amorphous Silica	1.0–5.0	SiO_2
		Titanium Dioxide	1.0–10	TiO_2
	Pink (PK)	Titanium Dioxide	1.0–10	TiO_2
	White (WH)	Titanium Dioxide	1.0–10	TiO2

The experiment continued into X-ray scanning process using μXCT (Rigaku nano3DX) with tube voltage at 50 kV, and tube current 24 mA, using L1080 lens (F.O.V φ3.6 (diameter) × 2.8 (height) mm), and X-ray target was Mo. The dimension of the X-ray specimens was cut into 10 x 50 x 1.3 mm to fit the F.O.V of the L1080 lens. After the completion of the image acquisition, the CT reconstruction processes were implemented using the computer connected with the apparatus and thus 1234 16-bit gray-scale tomograms with the resolution of 1648 × 1648 (2.2 μm/pixel) were obtained.

The quantitative analysis was performed using ImageJ and VGStudio software with processing the image obtained. The determination of tangential axis (5 lines) and longitudinal axis (6 lines) was carried out using VGStudio software with 3D image explained in Figure 1. After the image cutting, the grey value was analyze using ImageJ to determine the penetration distance.

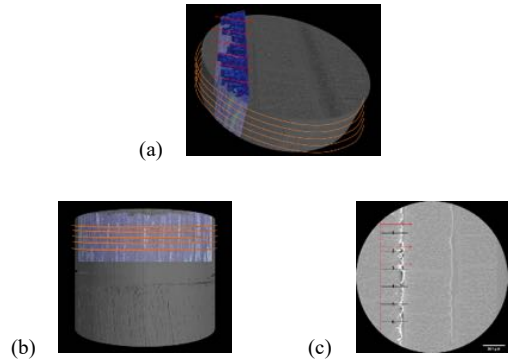

Fig. 1 The mechanisms of partition of the wood-coated samples (a) The determination of vertical and horizontal axis; red arrow indicates the longitudinal cut and orange line indicates the tangential cut of wood-coated surface; (b) tangential cut; (c) longitudinal cut

RESULTS AND DISCUSSION

The µXCT was applicable to visualize the coating penetration into the wood and distinguish between the woody material of Japanese beech veneer and the coating. The high-resolution image in 2D and 3D made it possible to quantify the coating penetration in three dimensionally. The existed of the coating were marked by the white line on the veneer and white dots in the veneer (Fig 2).

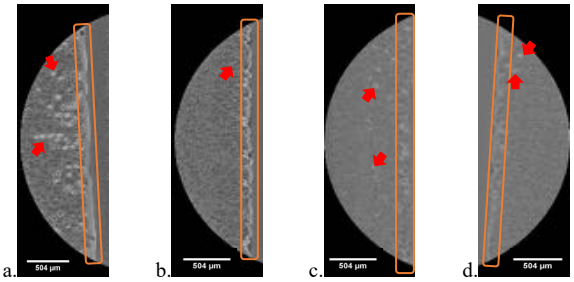

Fig 2. X-ray image of Japanese beech applied by (a) white coating; (b) matte white coating; (c) brown coating; (d) pink coating. (red arrow): white dots; (orange line): coating line.

The coating that used has the same active content (TiO_2) showed different penetration phenomenon and penetration amounts (Fig 3). The deepest coating penetration amount was found in white coating sample in accordance with its X-ray image results in Fig 2, whereas the other coating samples had shallower penetration. This could be caused by the concentration used by the chemical constituents of the coating which will affect the anchoring and penetration power of the coating. The different concentration of the chemical content could be caused the different viscosity level among the coatings. In addition, the anatomy of the wood used has different porosity and absorption even though was cut from the same veneer. In accordance with Žigon et al. (2021) stated that the adhesion of coatings to wood depends mainly on the diffusion and penetration of the liquid coating into the porous structure of the wood substrate.

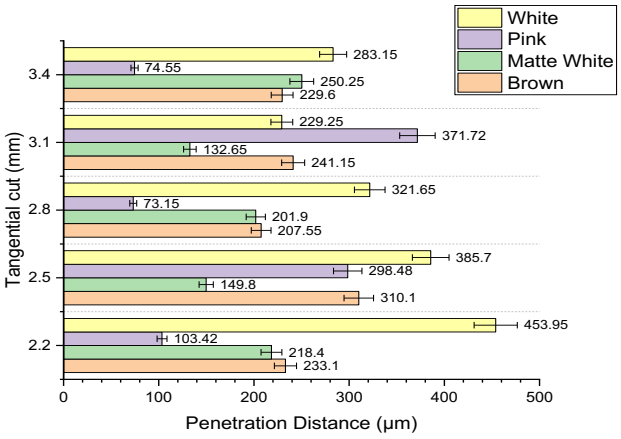

Fig 3. Average penetration amount of Japanese commercial coatings (Tangential cut)

In conclusion, the use of µXCT visualization can investigate the penetration of Japanese commercial coatings in the veneer and quantify its penetration amount. This finding is important for industrial aspects that might combine many wood species and coating products.

ACKNOWLEDGMENTS

The authors express their appreciation to JSPS KAKENHI for funding (Fund No.: 20K06163).

REFERENCES

Cassens DL and Feist WC (1986) Finishing Wood Exteriors. Forest Service Press., United States.

Dilik T, Koc KH, Hazir E and Erdinler ES (2014) Surface treatment, layer thickness and surface performance relations of wood materials. Proceedings of the 57th International Convention of Society of Wood Science and Technology. DOI: 10.13140/RG.2.1.3082.4488.

Ekaputri TS, Apsari NA and Tanaka T (2021) Visualization of commercial coating penetration into Fagus crenata blume wood using a non-destructive X-ray microtomography. Coatings, 11: 927.

Hazir E and Koc KH (2019) Evaluation of wood surface coating performance using water based, solvent based, and powder coating. Maderas., 21: 467–480.

Hazir E and Koc KH (2021) Evaluation of wood-based coating performance for ultraviolet roller and conventional air-atomization process. Maderas, 23: 1–10.

Meijer M, Thurich K and Militz H (1998) Comparative study on penetration characteristics of moderm wood coatings. Wood Science and Technology, 32: 347–365.

Žigon J, Pavlič M, Petrič M and Dahle S (2021) Surface properties of coated MDF pre-treated with atmospheric plasma and the in-fluence of artificial weathering. Mater. Chem. Phys., 263: 0254–0584.

Effects of Transglutaminase on Retrogradation of Wheat Flour

Dang Thi Kim Lien[1] and Takahisa Nishizu[2]

[1] The United Graduate School of Agricultural Science, Gifu University, 1-1 Yanagido, Gifu-shi, Gifu 501-1193, Japan
[2] Faculty of Applied Biological Sciences, Gifu University, 1-1 Yanagido, Gifu-shi, Gifu 501-1193, Japan

INTRODUCTION

Recently, the application of Transglutaminase (TG) in the food industry has notably increased, especially in wheat-based products. TG modifies proteins in wheat flour (WF), thereby improving both the product properties and the flour processability. In wheat-based products, retrogradation is a primary quality assessment criterion. The enzymatic activity of TG might influence this process. Consequently, it is essential to understand how TG impacts WF during heating and storage.

Retrogradation involves the crystallization of amylose and amylopectin in gelatinized starch as it cools, affecting the texture and shelf life of starch-based foods. Besides starch, protein in WF strongly affects the retrogradation process. Studies indicate that protein and its nature could promote or inhibit the retrogradation process (Chang et al., 2021).

TG is protein-glutamine γ-glutamyl-transferase (*EC 2.3.2.13*) that catalyzes the cross-linking reaction through an acyl transfer of glutamine and lysine. By modifying protein structure and changing its interaction with other components, TG can alter the physical and functional properties of protein in WF (Bauer et al., 2003a, 2003b). Specifically, TG reaction could modify protein molecular weight and its hydrophobicity, thus could possibly affect the WF properties during gelatinization and storage. However, scientific literature lacks substantial evidence regarding the impact of TG on starch properties during cooking and storage of WF.

This study aims to evaluate the effect of TG on WF by examining flour microstructure changes, thermal behaviors during gelatinization, and starch retrogradation after storage. The goal is to understand the TG and WF interaction to optimize its use in starchy foods.

MATERIALS AND METHODS

Materials: —WF contained 13.7% protein (dry weight) (Nippn Co., Japan) was purchased from a local supermarket. *Activa@ TG-K* containing 1% microbial Transglutaminase was provided by Ajinomoto Co. (Tokyo, Japan).

Purification of TG: Two grams of *Activa@ TG-K* was dissolved in 10 ml of 0.1 M Tris/HCl buffer (pH 7.5). The mixture was centrifuged at 15,000 rpm at 4°C for 30 mins. The supernatant was collected and dialyzed at 4°C for 6 hrs in Tris/HCl buffer (pH 7.5), changing the buffer every 2 hours. The final solution was a 0.2% TG solution.

Sample preparation: — Each sample was prepared by mixing 15 g of WF with 45 g of water in a 200 ml beaker, resulting in a 25% (w/w) solid WF suspension. TG was added at concentrations of 0%, 0.04%, 0.05%, and 0.06% (w/w) relative to the protein content (coded as Control, TG0.04, TG0.05, and TG0.06, respectively). The mixture was stirred for 30 minutes at 160 rpm in a water bath maintained at 50°C. After treatment, samples were cooled in ice for 5 mins and kept at 4°C to inhibit enzyme activity for microstructure observations by Confocal Scanning Laser Microscopy (CSLM*)*. For DSC and swelling power, samples were freeze-dried for 3 days and powdered. For XRD, samples were steamed at 104°C for 30 minutes, stored at 4°C for up to 7 days, then lyophilized and sieved to 100-µm for testing.

Swelling power (SP): —SP was conducted using a modified method from Konik-Rose et al. (2001). 40 mg WF and 1 ml water were mixed in a 1.5 ml centrifuge tube. After mixing, it was heated at 92.5 °C for 30 min with regular inversion. After colling and centrifugation, the supernatant was discarded, and residue weight determined the SP: ***SP* = Weight of residue / Dry weight of sample**

Differential scanning calorimeter (DSC): — 8.00 mg sample with triple its weight in distilled water were added in an aluminum pan. Measurement was conducted by a DSC (7000X, Hitachi, Japan) from 25-100°C at 2 °C/min. An empty pan (40 mg) was used as the reference.

RD by X-ray diffractometer (XRD):— XRD was used to measure RD as detailed by Taguchi et al. (2023). Wheat gel powder was added with 0.8% Zinc Oxide and 70% water before testing. The SmartLab XRD (Rigaku Co., Japan) was used at 45 kV and 200 mA, scanning at 2°/min between 10–37°. RD was determined by a given equation.

$$\mathbf{RD} = A_{17°}/A_s$$

Where $A_{17°}$ and A_s are the areas of the peaks near $2\theta \approx 17°$ and the zinc-oxide peak ($2\theta \approx 37°$), respectively.

RESULTS

Microstructure by CLSM: —The results from microstructure observation indicated binding tendency of starch granule to protein network in TG treatment. The protein network in TG sample was covered by starch granules while control sample did not show this phenomenon (Picture was presented in poster section).

Swelling power: — SP of TG sample was showed in Fig 1. Samples with TG treatment had lower SP value compared to control sample. SP value also presented for water adsorption of starch granule during heating. In this experiment, TG inhibited the water adsorption of wheat starch, especially at the enzyme concentration of 0.05%.

Thermal properties (DSC): —The data revealed alterations in gelatinization enthalpy (ΔH) without affecting gelatinization temperatures. The adding of TG

did not lead to the change in the starch gelatinization temperature, suggesting the starch structure remained unaltered (data not shown). However, a significant increase in *ΔH* was observed upon the addition of TG at concentrations of 0.05% and 0.06% (showed in Fig 1)

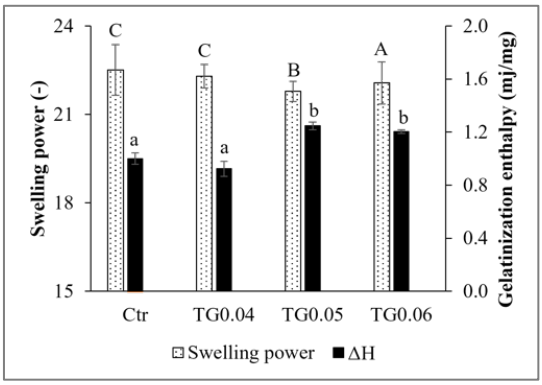

Fig. 1: Swelling power and gelatinization enthalpy of samples. TG0.04, TG0.05, and TG0.01 are samples with 0.04, 0.05, and 0.06%bTG (w/w of protein) respectively. Different letters indicate significant differences ($p \leq 0.05$).

Retrogradation of stored wheat gel (XRD): — The RD observed in samples treated with TG was lower compared to the control after storage, as showed in Fig 2. The RD increased along with the long period of storage in all samples. The addition of TG at 0.05% had a significant inhibitory effect on the retrogradation of WF.

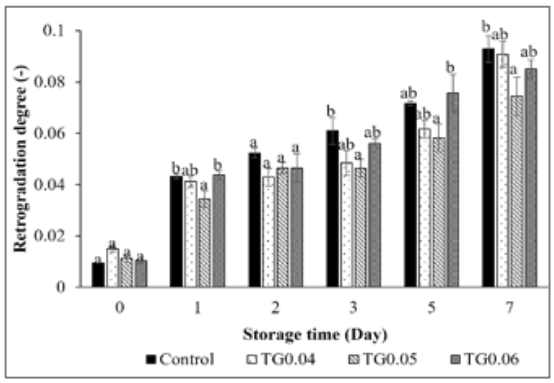

Fig. 2: Retrogradation degree of samples after 7 days of storage at 4ºC. Different letters indicate significant differences ($p \leq 0.05$). TG0.04, TG0.05, and TG0.01 are samples with 0.04, 0.05, and 0.06% TG (w/w of protein) respectively.

DISCUSSION

Integrating all the findings, it can be inferred that TG impact on the protein network restricts water absorption, modifies thermal properties of wheat starch, and subsequently influences starch retrogradation behavior during storage.

In Fig 1, we observe a decrease in swelling and an increase in *ΔH* with the addition of TG. As starch granules absorb water and start to swell, they experience a phase transition. The energy required to facilitate this transition and break the hydrogen bonds in the crystalline areas is termed the gelatinization enthalpy. The energy required to facilitate this transition and break the hydrogen bonds in the crystalline regions is termed the gelatinization enthalpy. If the penetration of water is hindered, starch granules cannot swell effectively. The limited swelling in the TG sample is caused by the protein network formation around the starch granules, which prevents full crystalline disruption. Therefore, more energy is required to disrupt this additional region. As a result, the *ΔH* in TG0.05 and TG0.06 increased accordingly.

The retrogradation reduction by TG treatment is possibly due to the reinforcement of protein network, which subsequently decreases SP and minimizes amylose leaching during gelatinization. This delay in amylose recrystallization consequently reduces the RD of wheat starch (Fig 2). Furthermore, the data also suggests a concentration-dependent effect of TG, with the optimal concentration being approximately 0.05%.

In conclusion, the result obtained from this study confirmed the application of TG has a significant impact on reducing starch retrogradation in WF. These findings underscore the significant potential and benefits of incorporating TG into the production of wheat-based products to improve overall quality.

REFERENCES

Basman A, Köksel H and Ng PK (2002) Effects of increasing levels of transglutaminase on the rheological properties and bread quality characteristics of two wheat flours. European Food Research and Technology, 215, 419–424.

Bauer N, Koehler P, Wieser H and Schieberle P (2003a) Studies on effects of microbial transglutaminase on gluten proteins of wheat. I. Biochemical Analysis. Cereal Chemistry, 80(6), 781–786.

Bauer N, Koehler P, Wieser H and Schieberle P (2003b) Studies on effects of microbial transglutaminase on gluten proteins of wheat. II. Rheological Properties. Cereal Chemistry, 80(6), 787–790.

Chang Q, Zheng B, Zhang Y and Zeng H (2021) A comprehensive review of the factors influencing the formation of retrograded starch. International Journal of Biological Macromolecules, 186, 163–173.

Konik-Rose CM, Moss R, Rahman S, Appels R, Stoddard F and McMaster G (2001) Evaluation of the 40 mg Swelling Test for Measuring Starch Functionality. Starch - Stärke, 53(1), 14–20.

Ogilvie O, Roberts S, Sutton K, Larsen N, Gerrard J and Domigan L (2021) The use of microbial trans-glutaminase in a bread system: A study of gluten protein structure, deamidation state and protein digestion. Food Chemistry, 340, 127903.

Taguchi T, Onishi M, Katsuno N, Miwa N, Oomoto C, Sato M, Sekita M, Yamaguchi H, Imaizumi T and Nishizu T (2023) Evaluation of starch retrogradation by X-ray diffraction using a water-addition method. LWT, 173, 114341.

Carotenoid Metabolism is Involved in the Granulation of Citrus 'Harumi' Fruit During Postharvest Storage

Zhiwei Deng[1,2], Gang Ma[2], Lancui Zhang[2], Daiki Kurata[2], Keisuke Nonaka[3], Fumitaka Takishita[3] and Masaya Kato[2,*]

[1] The United Graduate School of Agricultural Science, Gifu University, Gifu, Japan
[2] Department of Bioresource Sciences, Faculty of Agriculture, Shizuoka University, Shizuoka, Japan
[3] Institute of Fruit Tree and Tea Science, National Agriculture and Food Research Organization (NARO), Okitsu, Shizuoka, Japan

INTRODUCTION

Juice sacs granulation is a serious physiological disorder of citrus fruit that often occurs during postharvest storage. This granulation causes the colorless of the juice sacs, resulting in the loss of marketable values. The lignin content in the juice sacs is an important indicator for evaluating granulation. Moreover, carotenoids are the major pigments accumulated in citrus fruit, and their contents and compositions are crucial indicators for assessing citrus commercial and nutritional values of citrus fruit (Ma et al., 2021). However, the molecular mechanisms underlying the carotenoid accumulation in granulated fruit have not been clarified so far. In the present study, to elucidate the mechanism of granulation, we investigated the granulation rating, lignin content, and carotenoid metabolism during the granulation process in different sizes of 'Harumi' fruit.

MATERIALS AND METHODS

'Harumi' fruit originated from a hybrid between 'Kiyomi' tangor (*Citrus unshiu* × *C. sinensis*) and Ponkan (*C. reticulata* mandarin) were harvested from NARO (Shizuoka). According to the fruit size, the fruit were divided into two groups: S fruit (transverse diameter of 5.0 - 6.5 cm) and L fruit (transverse diameter of 8.5 - 10.0 cm). The fruit were stored at 10 ˚C for five months under 80 - 90 % RH. The degree of granulation was assessed according to the method of Hofman (2010). Lignin was extracted using the spectrometer method described by Li et al. (2022). The carotenoids were extracted following Kato's methods and measured by HPLC (Kato et al., 2004). Total RNA was extracted by using the phenol-chloroform method (Kato et al., 2004). The reaction mixture of Real-Time PCR was made according to the previous method (Ma et al., 2021).

RESULTS AND DISCUSSION

Granulation rating and lignin content — In this study, we found that the granulation rating of L fruit increased rapidly from the first month. Moreover, the lignin content in L fruit increased rapidly from the first month after harvest. In contrast, the lignin content slightly increased in the juice sacs of S fruit after harvest, in which no obvious granulation occurred during the storage period.

Previous studies indicate that the lignin content is inevitably increased in the granulated juice sacs, and the overaccumulation of lignin is an essential step in the granulation process. The lignin content in the juice sacs was increased by 1.5 to 5-fold in the granulated fruit of 'Ponkan' mandarin, 'Sanhongmiyou' pomelo, and navel orange (Huang et al., 2023).

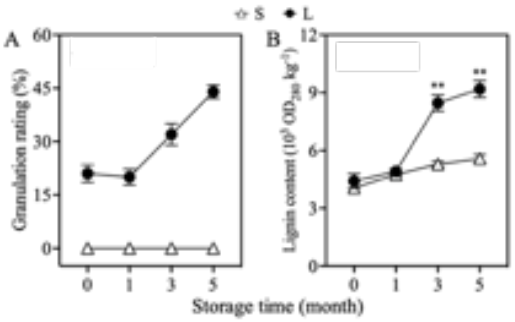

Fig. 1: Changes in the granulation rating (A) and lignin content (B) in the juice sacs of the S and L 'Harumi' fruit during the storage period.

Carotenoid contents — Carotenoids are an important quality index of citrus fruit. As the loss of orange color is a typical characteristic of granulated juice sacs, the changes in carotenoid contents are an important indicator of granulation, which could be used to predict the degree of granulation in citrus fruit. El-Zeftawi (1978) found that granulated juice sacs accumulated fewer carotenoids than healthy juice sacs in Valencia orange. The results in this study showed that S fruit accumulated more carotenoids than L fruit in the juice sacs. Moreover, the contents of β-cryptoxanthin, β-carotene, all-*trans*-violaxanthin, and 9-*cis*-violaxanthin in S fruit continued increasing after harvest, and the orange color of the juice sacs deepened gradually during the storage period. In L fruit, in contrast, the contents of β-cryptoxanthin, all-*trans*-violaxanthin, and 9-*cis*-violaxanthin decreased when the granulation aggravated in the third week after harvest, which led the juice sacs color to turn yellowish. These results indicated that the occurrence of granulation inhibited carotenoid accumulation and coloration in the juice sacs of L fruit in 'Harumi'

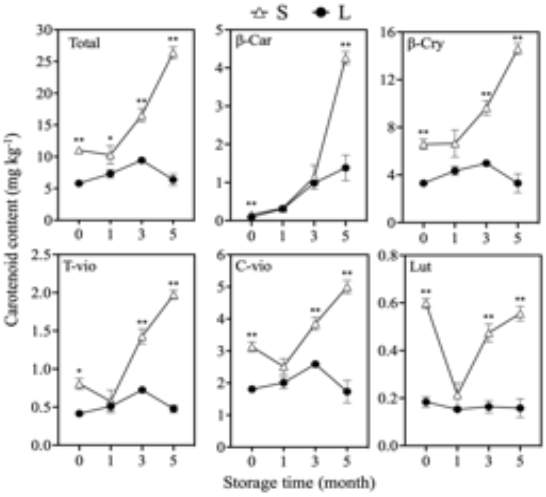

Fig. 2: Changes in the carotenoid content in the juice sacs of S and L fruit during the storage period.

Expression of carotenoid metabolism genes — To explore the molecular mechanism that causes the loss of orange color in the granulated juice sacs, the changes in the expression of carotenoid metabolic genes were investigated in this study. Genes expression showed that the modification of carotenoid accumulation was highly regulated at the transcriptional level in the granulated fruit. The expression of carotenoid biosynthetic genes CitPSY, *CitPDS*, and *CitZEP* increased with a peak at the first month in S fruit after harvest, while it decreased rapidly in L fruit during the storage period. Moreover, the expression of *CitLCYb2* and *CitHYb*, which are the key genes responsible for the β-cryptoxanthin biosynthesis, was higher in S fruit than in L fruit during the storage period. The changes in the gene expression suggested that carotenoid biosynthesis was inhibited in the granulated fruit of 'Harumi'. In addition, ABA is a downstream of metabolite of carotenoid, which is synthesized from the cleavage of 9-*cis*-violaxanthin and 9′ -*cis*-neoxanthin catalyzed by NCEDs. In this study, the results showed that the gene expression levels of *CitNCED2* and *CitNCED3* were higher in L fruit than in S fruit. The high expression of ABA biosynthetic genes and low content of ABA precursor in L fruit indicated that ABA biosynthesis was activated during the granulation process. The positive relationship between ABA and granulation was also reported in blood orange, in which ABA content increased in the granulated fruit (Hou et al., 2022). In this study, we found that the activation of ABA biosynthesis was accompanied by the enhancement of lignin content in the granulated fruit, which indicated that endogenous ABA triggered the lignin biosynthesis during the granulation process in L fruit of 'Harumi'.

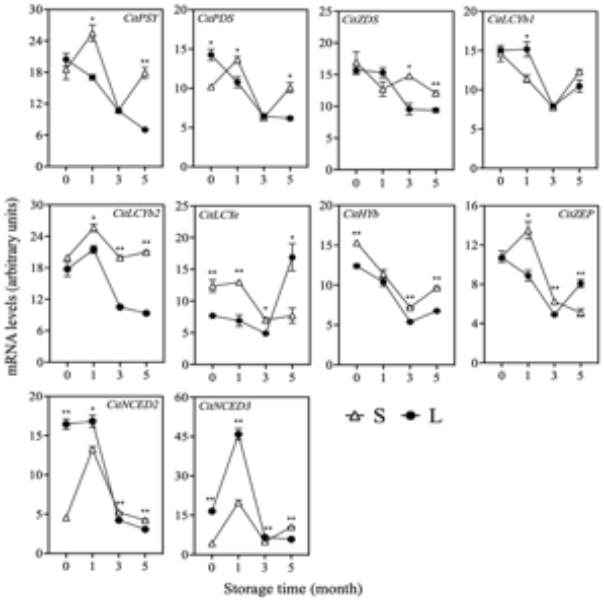

Fig. 3: Changes in the expression of carotenoid metabolism genes in the juice sacs of S and L fruit during the storage period.

REFERENCES

El-Zeftawi BM (1978) Factors affecting granulation and quality of late-picked Valencia oranges. J. Hortic. Sci., 53 (4): 331–337.

Hou J, Yan D, Huang M, Zeng K and Yao S (2022) Alteration of pectin metabolism in blood orange fruit (*Citrus sinensis* cv. Tarocco) in response to vesicle collapse. Food Qual. Saf., 6: fyac050.

Huang C, Hou J, Huang M, Hu M, Deng L, Zeng K and Yao S (2023) A comprehensive review of segment drying (vesicle granulation and collapse) in citrus fruit: Current state and future directions. Sci. Hortic., 309: 111683.

Kang C, Cao J, Wang Y and Sun C (2022) Advances of section drying in citrus fruit: The metabolic changes, mechanisms and prevention methods. Food Chem., 395: 133499.

Kato M, Ikoma Y, Matsumoto H, Sugiura M, Hyodo H and Yano M (2004) Accumulation of carotenoids and expression of carotenoid biosynthetic genes during maturation in citrus fruit. Plant Physiol., 134 (2), 824–837.

Li Q, Yao S, Deng L and Zeng K (2022) Changes in biochemical properties and pectin nanostructures of juice sacs during the granulation process of pomelo fruit (*Citrus grandis*). Food Chem., 376: 131876.

Ma G, Zhang L, Kudaka R et al. (2021) Exogenous application of ABA and NAA alleviates the delayed coloring caused by puffing inhibitor in citrus fruit. Cells, 10 (2): 308.

Correlation Between Soil Bacterial Communities and Nutrient Status in Tea Plants

Shuning Zhang[1], Naoki Yanagisawa[2], Mio Asahina[2], Hiroto Yamashita[2] and Takashi Ikka[1,2,3]

[1] The United Graduate School of Agricultural, Gifu University, 1-1 Yanagido, Gifu 501-1193, Japan
[2] Faculty of Agriculture, Shizuoka University, 836 Ohya, Shizuoka 422-8529, Japan
[3] Research Institute of Green Science and Technology, Shizuoka University, 836 Ohya, Shizuoka 422-8529, Japan

INTRODUCTION

Soil bacteria were attributed to be key biological indicators for assessing soil conditions, which directly participated in the soil nutrient cycle and rapidly responded in response to changes in the soil environment (Fierer and Jackson. 2006; Hermans et al. 2017). They also expanded the metabolic capacity of plants and participated in diverse processes including plant development, nutrient absorption, and stress responses (Bai et al. 2022). Soil pH has been shown to be the strongest factor affecting the diversity and composition of soil bacterial communities (Rousk et al. 2010). In addition, the rhizosphere was the important zone that direct interaction between roots and active microbes. It was also crucial to compare the differences between rhizosphere soil and bulk microbes.

Tea is known to thrive in an acid-tolerant environment, growing well in soil pH levels of 4-5. This unique soil environment encompasses various properties, nutrients, and microbes. However, it was insufficient to focus solely on the isolated effect of soil conditions on tea quality, as it overlooked the relationships between the belowground and aboveground components of tea plants. In this study, we emphasized the bacterial communities in tea soils from various tea plantations. Subsequently, we analyzed the nutrient status of tea plants, including their growth, tea quality, and essential mineral elements. Finally, we elucidated the interactions between soil microorganisms and tea plants. This allowed us to assess deeply the relationships between soil bacteria and tea nutrient status.

MATERIALS AND METHODS

The pot culture was conducted in the greenhouse at Shizuoka University (Shizuoka, Japan). One-year-old rooted tea cuttings of "Yabukita" were transplanted into Wagner pots. The five cultured soils were collected from one conventional soil and four fields with typical tea gardens in Shizuoka, and these soils were named soil A, B, C, D, and E respectively, which was according to the order of soil pH value (from the lowest to highest). In addition, each soil was set into two groups which named soil w/o plants (soil without tea plants in the pot) and soil with plants. All samples included rhizosphere soils, bulk soils, roots, stems, mature leaves, and new leaves. Soils were used to analyze bacterial communities using 16S rRNA sequencing, and some physicochemical properties. The nutrient contents of leaves and roots were followed by our laboratory-described methods including free amino acids (FAAs), catechins and caffeine, and mineral elements (Yamashita et al. 2020; Yamashita et al. 2021).

RESULTS AND DISCUSSION

To explore the difference in five soils from different pH ranges between core and noncore regions, we analyzed physicochemical indexes after a period of pot cultivation (Table 1). The results revealed that soil pH ranged between 3.31 and 6.37, with Carbon (C) to nitrogen (N) ratio (C/N) value ranging between 7.9 and 11.7, while there were no significant differences between soils with plants and soils w/o plants. In soils with inappropriate pH levels, tea leaves, both new and mature commonly exhibited mineral deficiencies. The concentrations of Ca, Mg, Fe and Al showed significant deficiency in new leaves. The tea growth was also inhibited in soil with higher pH levels.

The sequencing of soil bacterial communities showed that the species and diversity of bacterial communities in tea soils were higher than in soil without tea plants, indicating that tea plants could recruit a more abundant bacterial population (Fig. 1a). The principal coordinates analysis (PCoA) showed the points from the same soil types clustered closely and the cluster from different soil types separated clearly (Fig. 1b). The community analysis showed the most dominant bacterial phyla in tea soils were *Proteobacteria*, *Actinobacteria*, *Chloroflexi*, and *Actinobacteria*, while the most dominant families were *Acidobacteriaceae*, *Solirubrobacteraceae*, *Acetobacteraceae*, and *Mycobacteraceae* (Fig. 2). Based on the p-value and FDR value, key bacteria were screened and analyzed the relationships with tea quality and nutrient elements. The results showed that key families including *Micropepsaceae, Acidobacteriaceae* and *Microscillaceae* were found to actively participate in plant-microbe interactions (Fig.3).

CONCLUSIONS

Inappropriate soil pH results in growth inhibition and deficiency of various nutrients from tea leaves and roots. Exploring the intricate soil-microbe-plant interactions can help optimize nutrient management for high-quality tea. Further research will continue to track these key microbial

communities to understand their specific contributions to tea plants.

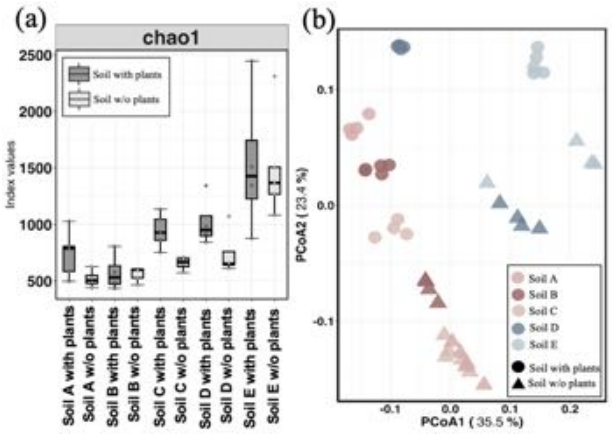

Fig. 1: The diversity of bacterial communities in soils from different pH conditions. (a) The α-Diversity (Chao1 index) of soil bacterial communities. (b) The β-Diversity (PCoA analysis) of soil bacterial communities.

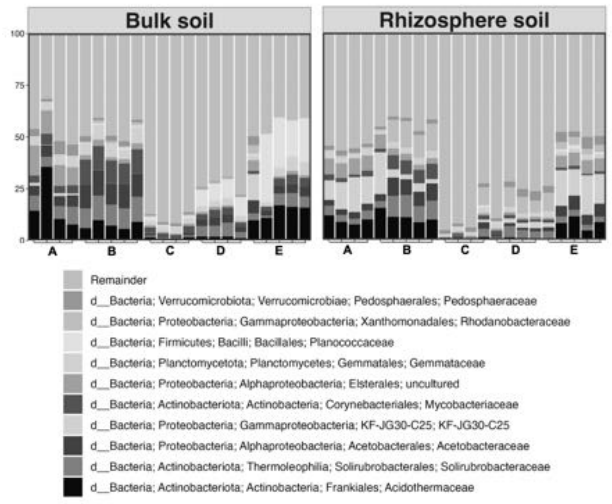

Fig. 2: The composition of bacterial communities in different soil types

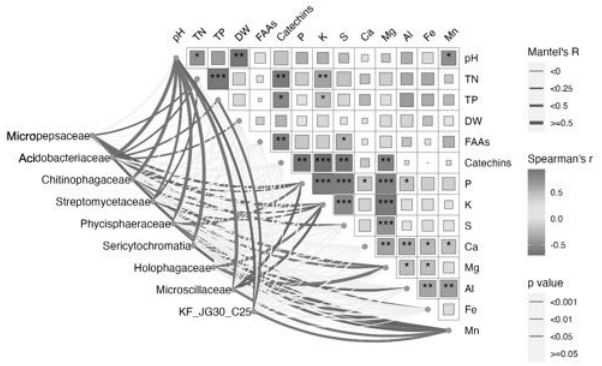

Fig. 3: Relationships between key bacteria and nutrient status in tea plants.

REFERENCES

Fierer N and Jackson RB (2006) The diversity and biogeography of soil bacterial communities. PNAs,103(3): 626–631.

Hermans SM, Buckley HL, Case BS, Curran-Cournane F, Taylor M and Lear G (2017) Bacteria as emerging indicators of soil condition. Applied and environmental microbiology, 83(1): e02826–16.

Bai B, Liu W, Qiu X, Zhang J, Zhang J and Bai Y (2022) The root microbiome: Community assembly and its contributions to plant fitness. Journal of Integrative Plant Biology., 64(2): 230–243.

Rousk J, Bååth E, Brookes P.C, Lauber C.L, Lozupone C, Caporaso J.G and Fierer N (2010) Soil bacterial and fungal communities across a pH gradient in an arable soil. The ISME journal, 4(10): 1340–1351.

Yamashita H, Fukuda Y, Yonezawa S, Morita A and Ikka T (2020) Tissue ionome response to rhizosphere pH and aluminum in tea plants (Camellia sinensis L.), a species adapted to acidic soils. Plant-Environment Interactions, 1(2): 152–164.

Yamashita H, Kambe Y, Ohshio M, Kunihiro A, Tanaka Y, Suzuki T and Ikka T (2021) Integrated metabolome and transcriptome analyses reveal etiolation-induced metabolic changes leading to high amino acid contents in a light-sensitive Japanese albino tea cultivar. Frontiers in Plant Science, 11, 611140

Table 1 Physicochemical properties in different soil types

Soil type		pH	EC (ms·cm-1)	Total P (mg/100g)	Total N (%)	Total C (%)	C/N
A	with plants	3.31±0.14f	0.23±0.04cd	1026.42±66.87d	3.70±0.11a	43.19±0.95a	11.70±0.58a
	w/o plants	3.48±0.06f	0.34±0.04a	1109.44±76.09cd	2.60±0.10a	41.97±0.76a	11.63±0.26a
B	with plants	3.73±0.10e	0.15±0.02e	1260.46±35.21b	2.58±0.20b	28.97±0.79bc	11.26±0.71a
	w/o plants	3.77±0.11de	0.16±0.02e	1274.92±43.37b	2.70±0.22b	29.73±0.34b	11.08±0.83ab
C	with plants	3.97±0.03cd	0.06±0.00f	643.26±27.39e	0.61±0.07d	6.87±0.82f	11.40±1.18a
	w/o plants	4.10±0.06c	0.07±0.00f	613.00±40.59e	0.52±0.06d	5.62±0.27f	10.78±0.94ab
D	with plants	4.72±0.12b	0.18±0.03de	1757.95±72.48a	3.45±0.23a	26.51±1.68d	7.87±0.23c
	w/o plants	4.59±0.12b	0.33±0.06ab	1870.30±79.14a	3.42±0.27a	26.85±1.97cd	7.86±0.21c
E	with plants	6.37±0.05a	0.27±0.03bc	1118.18±70.25cd	1.45±0.10c	14.66±0.65e	10.19±1.04ab
	w/o plants	6.49±0.14a	0.33±0.02ab	1173.16±63.02bc	1.44±0.12c	13.86±0.28e	9.69±0.62b

Evaluation of the Impact of Climate Change on River Temperature

Khadiza Akter Mousumi[1], Takeo Onishi[2], Ken Hiramatsu[2] and Toshifumi Imaizumi[3]

[1] The United Graduate School of Agricultural Science, Gifu University, 1-1 Yanagido, Gifu-shi, Gifu 501-1193, Japan
[2] Faculty of Applied Biological Sciences, Gifu University, 1-1 Yanagido, Gifu-shi, Gifu 501-1193, Japan
[3] Faculty of Agriculture, Shizuoka University, 286, Ohya, Suruga-ku, Shizuoka-shi, Shizuoka 422-8529, Japan

INTRODUCTION

In aquatic ecosystems, river temperature is a crucial indicator of biodiversity and sustainability. River discharge and water temperature directly affect water quality (Ducharne 2008; Haag and Westrich 2002; Ozaki et al. 2003), the growth rate and distribution of freshwater organisms (Eaton and Scheller 1996; Ebersole et al. 2001; Mohseni et al. 2003). The dynamics and kinetics of biochemical reactions are influenced by river temperature, which also affects the availability, behavior, and kind of aquatic species in the ecosystem to which it belongs. The availability and temperature of water are also economically important, for example for thermoelectric power production (Forster and Lilliestam 2011; Koch and Vo¨gele 2009; Manoha et al. 2008), drinking water production (Ramaker et al. 2005; Senhorst and Zwolsman 2005), fisheries (Bartholow 1991; FAO 2008; Ficke et al. 2007) and recreation (EEA 2008b; Webb et al. 2008). Climatic conditions have a strong influence on water temperature. The increase in stream temperatures has already been observed in many countries., including Austria (Webb and Nobilis 1994), China (Chen et al. 2016), Germany (Arora et al. 2016), Poland (Kedra and Wiejaczka 2018; Graf and Wrzesinski 2020), UK (Orr et al. 2015), Switzerland (Michel et al. 2020) or USA (Kaushal et al. 2010; Seekell and Pace 2011; Isaak et al. 2018). Changes to natural water temperature regimes can result in myriad effects on aquatic organisms, water quality, circulation patterns, recreation, industry, and utility operations. Consequently, livelihood of the inhabitants depending on the river will also change. So, tracking changes in water temperature is key to better understanding the potential effects of global climate change on freshwater ecosystems.

Predicting the impact of climate change on river systems is imperative for effective management of aquatic ecosystems. This study will demonstrate the potential impact of climate on rivers temperature and how this might affect the future ecological systems. The objectives of the study are:

- To evaluate the processes involving climatic, hydrologic, and their interactions that determine the stream temperature.
- To investigate the impact of air temperature and streamflow changes on river temperature.
- To investigate the effect of changing temperature on aquatic ecosystem.
- To determine the influence of changing stream temperature on water quality, habitats of river and on the lifestyle of people.
- To find the best way to mitigate climate change and to adapt with the changing situation
- To develop long-term strategies and management policies to match with climate change phenomenon.

MATERIALS AND METHODS

The study site for this research is Nagara river. The Nagara River has its source in the city of Gujō, Gifu Prefecture, and its mouth in the city of Kuwana, Mie Prefecture, Japan. With a length of 166 km (103 mi), it drains an area of 1,985 square kilometres (766 sq mi) in the Chūbu region and empties into Ise Bay. To evaluation climate change impacts on the study site the dataset of the following website will be used.

http://www.miroc-gcm.jp/~pub/d4PDF/index_en.html

Present and future climate data will be generated by using a regional climate mode through dynamic downscaling approach. In this study, a watershed hydrology model, Soil and Water Assessment Tool (SWAT) will be utilized to simulate flow which is developed by the United States Department of Agriculture (USDA) and one of the most widely used simulators for hydrologic modelling (Arnold et al. 2012). It is a semi-distributed hydrological simulator used to simulate several processes over an extended period, primarily in rural catchments (Arnold et al. 1998). The SWAT model has been extensively applied to various problems such as land cover changes, agricultural management, and climate changes. The several input data and their sources are given in the following table:

Table 1: Input data for SWAT and their sources

Data	Source
DEM	https://asterweb.jpl.nasa.gov/
Land use	https://www.eorc.jaxa.jp/ALOS/en/dataset/lulc_e.htm
Soil type	https://www.mlit.go.jp/en/
Discharge	http://www1.river.go.jp/

River temperature data will be observed in the research project '水防災・農地・河川生態系・産業への複合的な気候変動影 響と適応策の研究', which is funded by The Environment Research and Technology Development Fund of the Ministry of Environment.

EXPECTED RESULTS

- The results of the study will provide tool(s) that will determine the climate change effects on river temperature.
- The findings of the study will show the effects of changing river temperature on aquatic ecosystems.
- The results of this study can be very useful in water resource planning, effective management of aquatic ecosystems.

REFERENCES

Arnold JG, Srinivasan R, Muttiah RS and Williams JR (1998) Large area hydrologic modeling and assessment part I: model development. Journal of the American Water Resources Association, 34 (1): 73–89.

Arnold JG et al. (2012) SWAT: model use, calibration, and validation. American Society of Agricultural and Biological Engineers, 55 (4): 18.

Arora R, Tockner K and Venohr M (2016) Changing River temperatures in northern Germany: trends and drivers of change. Hydrological Processes, 30(17): 3084–3096.

Bartholow JM (1991) A modeling assessment of the thermal regime for an urban sport fishery. Environmental Management, 15: 833–845.

Chen D, Hu M, Guo Y and Dahlgren RA (2016) Changes in river water temperature between 1980 and 2012 in Yongan watershed, eastern China: Magnitude, drivers, and models. Journal of Hydrology, 533: 191–199.

Ducharne A (2008) Importance of stream temperature to climate change impact on water quality. Hydrology and Earth System Sciences, 12(3): 797–810.

EEA (2008b). Impacts of Europe's Changing Climate – Indicator-based Assessment. EEA, Copenhagen.

Eaton JG and Scheller RM (1996) Effects of climate warming on fish thermal habitat in streams of the United States. Limnology and oceanography, 41(5): 1109–1115.

Ebersole JL, Liss WJ and Frissell CA (2001) Relationship between stream temperature, thermal refugia and rainbow trout Oncorhynchus mykiss abundance in arid‐land streams in the northwestern United States. Ecology of freshwater fish, 10(1): 1–10.

FAO (2008) Climate Change Implications for Fisheries and Aquaculture. FAO, Rome, Italy, p. 41.

Ficke AD, Myrick CA and Hansen LJ (2007) Potential impacts of global climate change on freshwater fisheries. Reviews in Fish Biology and Fisheries, 17: 581–613.

Forster H and Lilliestam J (2011) Modeling thermoelectric power generation in view of climate change. Regional Environmental Change, 4: 327–338

Graf R and Wrzesiński D (2020) Detecting patterns of changes in river water temperature in Poland. Water, 12(5).

Haag I and Westrich B (2002) Processes governing river water quality identified by principal component analysis. Hydrological processes, 16(16): 3113–3130.

Isaak DJ, Luce CH, Chandler GL, Horan DL and Wollrab SP (2018) Principal components of thermal regimes in mountain river networks. Hydrology and Earth System Sciences, 22(12): 6225–6240.

Kaushal SS, Likens GE, Jaworski NA, Pace ML, Sides AM, Seekell D, Belt KT, Secor DH and Wingate RL (2010) Rising stream and river temperatures in the United States. Frontiers in Ecology and the Environment, 8(9): 461–466.

Koch H and Vo¨gele S (2009) Dynamic modelling of water demand, water availability and adaptation strategies for power plants to global change. Ecological Economics, 68: 2031–2039.

Kędra M and Wiejaczka Ł (2018) Climatic and dam-induced impacts on river water temperature: Assessment and management implications. Science of the Total Environment, 626: 1474–1483.

Manoha B, Hendrickx F, Dupeyrat A, Bertier C, and Parey S (2008) Climate change impact on the activities of Electricite de France. Houille Blanche-Revue Inter nationale De L Eau, 55–60.

Michel A, Brauchli T, Lehning M, Schaefli B and Huwald H (2020) Stream temperature and discharge evolution in Switzerland over the last 50 years: annual and seasonal behaviour. Hydrology and Earth System Sciences, 24(1): 115–142.

Mohseni O, Stefan HG and Eaton JG (2003) Global warming and potential changes in fish habitat in US streams. Climatic change, 59(3): 389–409.

Orr HG, Simpson GL, des Clers S, Watts G, Hughes M, Hannaford J, Dunbar MJ, Laizé CL, Wilby RL, Battarbee RW and Evans R (2015) Detecting changing river temperatures in England and Wales. Hydrological Processes, 29(5): 752–766.

Ozaki N, Fukushima T, Harasawa H, Kojiri T, Kawashima K and Ono M (2003) Statistical analyses on the effects of air temperature fluctuations on river water qualities. Hydrological Processes, 17(14): 2837–2853.

Ramaker TAB, Meuleman AFM, Bernhardi L and Cirkel G (2005) Climate change and drinking water production in The Netherlands: a flexible approach. Water Science and Technology, 51: 37–44.

Seekell DA and Pace ML (2011) Climate change drives warming in the Hudson River estuary, New York (USA). Journal of Environmental Monitoring, 13(8): 2321–2327.

Senhorst HAJ and Zwolsman JJG (2005) Climate change and effects on water quality: a first impression. Water Science and Technology, 51: 53–59.

Webb BW and Nobilis F (1994) Water temperature behaviour in the river Danube during the twentieth century. Hydrobiologia, 291(2): 105–113.

Webb BW, Hannah DM, Moore RD, Brown LE and Nobilis F (2008) Recent advances in stream and river temperature research. Hydrological Processes, 22: 902–918.

Evaluating the Effect of Soil Clod Presence and Seeding Rate on Soybean Yield and Seedling Establishment Using Bayesian Multilevel Mediation Analysis

Luthfan Nur Habibi[1], Tsutomu Matsui[2] and Takashi S.T. Tanaka[2, 3]

[1] The United Graduate School of Agricultural Science, Gifu University, 1-1 Yanagido, Gifu-shi, Gifu 501-1193, Japan
[2] Faculty of Applied Biological Sciences, Gifu University, 1-1 Yanagido, Gifu-shi, Gifu 501-1193, Japan
[3] Artificial Intelligence Advanced Research Center, Gifu University, 1-1 Yanagido, Gifu-shi, Gifu 501-1193, Japan

INTRODUCTION

The yield of soybean (*Glycine max* (L.) Merr.) is affected by the interaction of multiple factors including genotype, environmental effect, and also management practices. This interaction created variation in the optimal yield-to-seeding rates, where the environment that have high yield tend to need lower seeding rates compared to in low-yielding environments (Carciochi et al. 2019; Corassa et al. 2018). Environmental factors could hinder the establishment of soybean seedling that can affect the final plant population.

In Japan, soil clods easily appeared in the field surface after heavy rain. Soil clods result from the interaction between soil organic matter, soil moisture, and particle size distribution. The existence of soil clods during the emergence stage can hinder seedling establishment, making it a limiting factor for plant population and final yield. Ideally, soil properties should be incorporated as covariates in crop yield response modeling, but destructive measurement of soil properties are costly for on-farm experimentation. Therefore, soil clods can be used as the proxy for soil properties data in crop yield response model. Remote sensing can be utilized to simultaneously assess soil clods and established seedling numbers using advanced segmentation algorithm based on deep learning technique.

The direct impact of soil properties on the final yield, apart from the indirect influence mediated by seedling establishment, can be evaluated by measuring soil clods. Bayesian multilevel mediation analysis can be used to estimate the direct and indirect effect between variables through mediator variable (Tofighi et al. 2013). This study aimed to investigate the interaction between soil clod presence, established seedling numbers, and final soybean yield using multilevel mediation analysis. Moreover, an on-farm experiment was conducted to assess the effects of different seeding rates on the seedling number and final yield.

MATERIALS AND METHODS

Experimental design and data collection—On-farm experiments were carried out in two soybean fields located in Kaizu City, Gifu. The experimental design was randomized strip trial with total of eight different seeding rates. The experiment then evaluated using data-driven yield prediction model with UAV-based imagery and weather data established using LASSO regression model with accuracy measurement of root mean square error of 51.96 kg ha^{-1} (Habibi et al. *in prep*). Yield within 3×3 m^2 grids were quantified for further data analysis.

Measurement of seedling establishment and soil clod—The number of established seedlings and soil clod percentage in field were evaluated using RGB imagery with YOLACT, a semantic segmentation algorithm. Images of the fields were taken using a Sony A-6400 camera mounted on a DJI Matrice 300. The images were captured specifically during the seedling emergence stage.

Model for measuring the number of established soybean seedlings was trained using 200 images with an average of 15 seedling annotations per image. The number of seedlings within 3×3 m² grids, corresponding to the yield observations, was counted. Meanwhile, the soil clods was measured using model trained with 70 images with an average of 350 soil clod annotations per image. Predicted soil clod with diameter larger than 2 cm were transformed into binary images. These binary images were overlaid with a grid of 3×3 m² polygons to extract the percentages of soil clod presence.

Multilevel mediation analysis—The 1-1-1 multilevel mediation model was presented in the following equations:

Level-1 models

$$seedling\ number_{ij} = a_{0j} + a_1 soil\ clod_i + e_{ij}$$
$$yield_{ij} = b_{0j} + b_1 seedling\ number_i + b_2 soil\ clod_i + f_{ij}$$

Level-2 models

$$a_{0j} = a_0 + u_{0j}$$
$$b_{0j} = b_0 + v_{0j}$$

Error terms

$$e_{ij} \sim N(0, \sigma_e^2)$$
$$f_{ij} \sim N(0, \sigma_f^2)$$
$$\begin{pmatrix} u_{0j} \\ v_{0j} \end{pmatrix} \sim N(0, \Sigma); \quad \Sigma = \begin{pmatrix} \sigma_{u_{0j}}^2 & \sigma_{u_{0j},v_{0j}} \\ \sigma_{u_{0j},v_{0j}} & \sigma_{v_{0j}}^2 \end{pmatrix}$$

where $yield_{ij}$ is the observed soybean yield (kg ha^{-1}) in the corresponding j seeding rate (the outcome), $seedling\ number_{ij}$ is the number of established seedlings in plot area (the mediator), $soil\ clod_i$ is the percentage of soil clod in plot area (the independent variable), a_{0j} and b_{0j} denote the intercepts of the mediator and outcome models for each seeding rate j, a_{1j} represent the effect of soil clod

presence on established seedling, b_{1j} signifies the effect of soil clod presence on soybean yield, and b_{2j} indicates the effect of established seedling number on yield while holding soil clod constant. The 1-1-1 multilevel mediation model scheme was presented in Fig. 1.

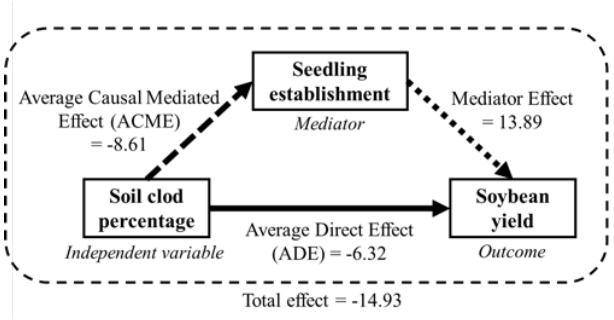

Fig. 1: The 1-1-1 multilevel mediation model scheme and results.

The average direct effect (ADE) of soil clod presence on yield was denoted by the b_2 value, whereas the average causal mediated effect (ACME) or the indirect effect was calculated by multiplying the a_1 and b_1 values. The mediator effect was represented by the b_1 value. The total effect was computed by summing up the direct and indirect effects. The proportion mediated was determined by dividing the ACME value by the total effect. The mediation analysis was carried out using the *mediation* feature provided by 'bayestestR' package in R. Bayesian estimation was performed using Markov chain Monte Carlo (MCMC) chains with 4000 saved iterations for the posterior inference. The Bayesian analysis was performed through the *stan_mvmer* feature available in 'rstanarm' package in R.

RESULTS AND DISCUSSION

Causal mediation analysis results—Soil clod presence had indirect effect to soybean yield through the seedling establishment by an average of -8.61 kg ha^{-1} per one percent increase under typical conditions (Fig. 1). The direct effect of soil clod appearance in the field had less impact than the mediated effect through seedling number. The total effect was estimated at -14.93 kg ha^{-1}.

Soil clods had a negative impact on yield performance through both direct and indirect relationships. Specifically, soil clods significantly influenced yield by affecting seedling numbers during the emergence stage. Soil clods presence could hinder seedling emergence as growing seedlings must overcome the soil impedance caused by the clods and soil compaction, which could result in seedling mortality (Gong et al. 2019).

Effect of seeding rates on seedling number and yield—The average established seedling number in the fields varied from around 6 to 9 plants m^{-2} depending on the seeding rate (data not shown). The field conditions had a significant impact on the average number of seedlings. The typical yield performance in both fields plateaued in approximately 110 kg ha^{-1} in the most optimized seeding rate setup in both fields.

Notable differences were observed in the established seedling numbers between the two fields. The use of larger seeds in Field 2 potentially contributed to better average seedling emergence. Planting high-vigor seeds and adjusting seed spacing and at optimum seeding rates during sowing can be implemented to ensure sufficient seedling numbers (Hyatt et al. 2007). Nonetheless, the yield performance of Field 1 exceeded that of Field 2 significantly at lower seeding rates. Consequently, it is crucial to optimize the seeding rate for each field according to agronomic knowledge of the yield response to environmental factors, rather than solely concentrating on the number of established seedlings.

In this study, soil clods measured using UAV imagery proved to be suitable proxies for soil property covariates when evaluating yield in on-farm experimentation studies. The higher presence of soil clod in field surface could reflect a lower water holding capacity or drainage capability, which directly affected the yield. Implementing water table management, including drainage and sub-irrigation systems, could offer a solution to mitigate soybean yield performance instability due to flooding or drought (Matsuo et al. 2018). Other factors during the latter growing stages that were not accounted in current study could also impact the yield. Additional research is required to consider the environmental effects on the soybean yield component and final yield, particularly during the pod initiation and seed-filling stages.

REFERENCES

Carciochi WD et al. (2019) Soybean seed yield response to plant density by yield environment in North America. Agron. J., 111: 1923–1932. https://doi.org/10.2134/agronj2018.10.0635

Corassa GM, Amado TJC, Strieder ML, Schwalbert R, Pires JLF, Carter PR and Ciampitti IA (2018) Optimum soybean seeding rates by yield environment in southern Brazil. Agron. J., 110, 2430–2438. https://doi.org/10.2134/agronj2018.04.0239

Gong H, Zeng Z and Qi L (2019) A discrete element model of seed-soil dynamics in soybean emergence. Plant Soil, 437, 439–454. https://doi.org/10.1007/s11104-019-04007-y

Hyatt J, Wendroth O, Egli DB and TeKrony DM (2007) Soil compaction and soybean seedling emergence. Crop Sci., 47, 2495–2503. https://doi.org/10.2135/cropsci2007.03.0171

Matsuo N, Yamada T, Takada Y, Fukami K and Hajika M (2018) Effect of plant density on growth and yield of new soybean genotypes grown under early planting condition in southwestern Japan. Plant Prod. Sci., 21, 16–25. https://doi.org/10.1080/1343943X.2018.1432981

Tofighi D, West SG and Mackinnon DP (2013) Multilevel mediation analysis: The effects of omitted variables in the 1-1-1 model. Br. J. Math. Stat. Psychol., 66, 290–307. https://doi.org/10.1111/j.2044-8317.2012.02051.x

Estimation of Metabolizable Energy Value of Okara Meal in Broiler Chicken Using Chick Bioassay, Approximate Nutritive Value, and *in Vitro* Digestibility Technique

Bagus Himawan Wicaksono[1], Norimatsu Marina[2] and Yamamoto Akemi[2]

[1] The United Graduate School of Agricultural Science, Gifu University, 1-1 Yanagido, Gifu 501-1193, Japan
[2] Faculty of Applied Biological Sciences, Gifu University, 1-1 Yanagido, Gifu 501-1193, Japan

INTRODUCTION

The investigation of cost-effective resources that offer similar nutritional value to commercial diet is great interest (Sugiharto 2022). Okara, also known as soybean by-product residue, is derived from the ruptured cotyledon cells of soybeans. Globally produced 14 million tonnes, yet half of the byproduct is discarded (Privatti & Rodrigues 2021). Dried okara has gained attention as a potential feed ingredient for broiler chickens. The crude protein (CP) of dried okara ranges from 22% to 40%, depending on the soybean variety and processing methods such as milling and heating (Sugiura et al. 2009). Although the CP is lower than soybean meal (SBM), okara has variable and relatively high levels of crude fiber (CF) between 12-20%, potentially interfere the feed digestion process in poultry (Diaz-Vargaz et al. 2016)

One of the key factors that determine the suitability of a feed ingredient for broiler chickens is metabolizable energy (ME) content (Edwards & Hemsworth, 2021). Studies have shown that dried okara has ME values ranging from 1572 to 2700 kcal per kilogram of dry matter (Diaz-Vargaz et al. 2016). Okara from soymilk residue contains higher nutritive value compared to the tofu residue (Toda et al. 2007), since the filtration process occurred once to obtain soymilk residue. Subsequently, higher filtration frequency affects lowering non-starch polysaccharides in CF (Olukosi et al. 2015), increasing nutrient digestibility. As results, ME values of dried okara are vary by these consequences. Due to this situation, inaccurate feed formulation might occur and lower the production efficiency of poultry.

The current ingredient databases provide insufficient nutritive value of okara, particularly in terms of its energy value as a poultry feed. It is indispensable to determine the precise nutritive and ME value, ensuring broilers obtained balanced rations both nutrient requirement as well as energy necessity. To promote the acceptance of okara as a poultry feedstuff, understanding of chemical components and okara's utilization in broiler meal are crucial to be undertaken. Thus, this research aims to determine ME and digestibility of six okara samples using chick bioassay, approximate nutritive value, and *in vitro* digestibility technique.

MATERIALS & METHODS

Okara Sampling—Dried okara samples were taken from various tofu and soymilk factory. There are six samples used in this experiment, four samples from tofu productions and two samples from soymilk processing.

Proximate Analysis—The levels of moisture content (MC), CP, crude ash (CA), and fat (Ether Extract or EE) were measured using AOAC (2006) methods. While the nitrogen-free extract (NFE) value acquired from subtraction of all proximate analysis parameter.

In Vivo (Chick Bioassay)—A total of 105 Chunky strain male broiler chicken 25-days-old were used. Okara's ME was evaluated by using the method of Kong & Adeola (2014). The amount of given feed was 89 g/chick/day. The last three-day of experiment, fecal or excreta were collected, dried in oven, and measured the gross energy (GE) using bomb calorimeter (Shimadzu, CA-4PJ).

In Vitro (Laboratory Assay)—The energy digestibility was determined using modified Furuya et al. (1979) methods. About 0.5 gram of samples were mixed with 10 ml of 20 mg pepsin/ml 0.0075M HCl solution (pH 2.0) in 100 ml flask. Each flask then gently shaked for 4h at 39ºC. Afterwards, about 10 ml of 50 mg/ml pancreatin (pH 6.8) was used, shaked in the same conditions. After centrifugation, sample was filtered and dried in oven before energy analysis. The digestibility values were examined using equation: [1 – (Residue/Sample) x 100].

Statistical analysis—Okara's nutritive value were examined using Pearson correlation. ME estimation were outlined using step-wise regression, while *in vivo* and *in vitro* digestibility correlation using linear regression.

RESULTS AND DISCUSSION

The results of this research shown that samples A, B, C, E, and F have high CP (>22%) which generally required in chicken diets in the first 4-weeks. However, only samples B and E that recommended for poultry feedstuff, specifically in terms of CF to be 8% or lower (Table 1). Sample E has features in moderate CA, highest amount of CP, low CF, lowest EE, and high NFE compared to all samples. Whereas, from tofu sources, sample B can be considered as secondary alternative feedstuff, referring the adequate CP level & low CF value.

Table 1: Nutrient compositions of okara as fed-basis

Samples	MC	CA	CP	CF	EE	NFE
Tofu						
A	4.6	5.3	22.6	11.3	14.7	46.3
B	4.4	5.5	25.2	8.2	17.7	43.4
C	8.8	4.6	24.9	17.4	20.0	33.1
D	7.6	6.2	16.1	20.3	13.9	43.5
Soymilk						
E	6.0	6.4	37.9	8.8	10.7	36.2
F	6.7	8.1	25.1	19.1	12.7	34.9

In vivo assay showed digestibility of various okara that were utilized as feedstuff, averagely accounted 59.5% digestibility. Four evaluated tofu okara samples showed similarity with Diaz-Vargaz et al. (2016), accounted for 2.7 Mcal/kg DM tofu okara. While the okara from soybean processing resulted higher ME. This is supporting Toda et al. (2007) study, stating that soymilk okara have higher nutritive value which resulting higher ME respectively. As a result, both GE and ME from two soymilk okara samples are higher compared to tofu okara. It can also be seen that higher digestibility value followed with higher CP combined against lower CF, specifically in soymilk okara (Table 1 and Table 2).

Table 2: *In vivo* energy digestibility of okara

Samples	ME (Mcal/kg DM)	GE (Mcal/kg DM)	Digestibility (%)
Tofu			
A	2.79	4.99	56.0
B	2.78	4.96	56.1
C	2.78	5.22	53.3
D	2.95	4.72	62.6
Soymilk			
E	3.30	5.10	64.8
F	3.30	5.12	64.5
Average	2.98	5.02	59.5
SD	0.25	0.17	5.0

Through the examined okara's nutritive value data, Pearson correlation showed that CA and EE were strongly related to apparent ME value. estimation of apparent ME equation using stepwise regression. Stepwise regression is a statistical method used in the context of multiple linear regression analysis, which aims to select the most relevant independent variables (predictors) for building a predictive model. Its primary goal is to choose a subset of predictors that best explain the variation in the dependent variable while minimizing overfitting.

Table 3: Estimated equation of apparent ME

Model	Predictors	Equation (Kcal/kg)	R^2	p-value
1	EE (X)	-69.60 X + 3960.45	0.72	0.032*
2	EE (X_1) NFE (X_2)	-66.54 X_1 – 27.32 X_2 + 5104.57	0.96	0.008*

In table 3, the equation are outlined into two models. Model one has moderate R^2 value, by only using EE data. Prediction of apparent ME by only using EE data resulting lower accuracy. Hence, the second model from stepwise regression are using EE and NFE data. Though the R^2 value is comprisingly high, acquiring NFE data was time-consuming.

Fig. 1 shows the relationship between *in vivo* and *in vitro* digestibility energy. Based on the linear regression, accuracy of *in vivo* and *in vitro* relationship equation is considered very low. Nutritional compositition of feedstuff supposed to be similar in order to obtain good equation (Furuya et al. 1979). As a result, the relationship between *in vivo* and *in vitro* digestiblities was different from one to another okara samples.

Based on this experiment, the preferred technique in estimating ME of okara feedstuff is using approximate nutritive value combined with step-wise regression. In case of other laying-hen feedstuff, study from Furuya et al. (1979) showed good relationship between *in vivo* and *in vitro* digestibility. While okara, this feedstuff could be unique, presuming the water absorption ability. Hence, estimation using *in vitro* technique require improvement for predicting okara's digestibility.

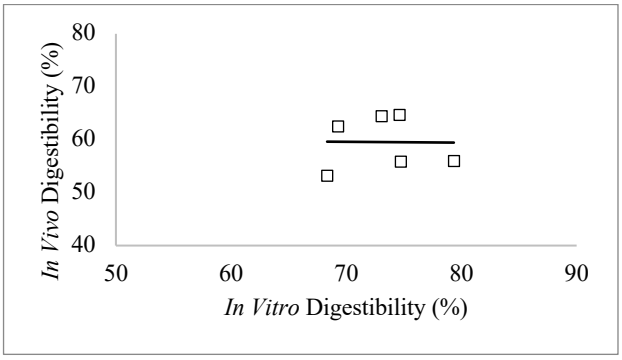

Fig. 1: Relationship between *in vivo* and *in vitro* digestibilities energy (□) of broiler chicken

REFERENCES

Diaz-Vargaz M, Murakami AE, Ospina-Rojas IC, Zanetti LH, Puzotti MM & Guerra AFQG (2016) Use of okara (aqueous extract reside) in the diet of starter broiler. Canadian Journal of Animal Science, 96: 416–424.

Edwards LE & Hemsworth PH (2021) The impact of management, husbandry and stockperson decisions on the welfare of laying hens in Australia. Animal Production Science, 61: 944–967.

Furuya S, Sakamoto K & Takahashi S (1979) A new in vitro method for the estimation of digestibility using the intestinal fluid of the pig. Br. J. Nutr., 41: 511–520.

Olukosi OA, Beeson LA, Engliyst K & Romero LF (2015) Effects of exogenous protease without or with carbohydrases on nutrient digestibility and disappearance of non-starch polysaccharides in Broiler Chickens. Poultry Science, 00: 1–8.

Privatti RT & Rodrigues CEDC (2021) An overview of the composition, applications and recovery techniques of the components of okara aimed at the biovalorization of this soybean processing residue. Food Reviews International, 29: 1–24.

Kong C & Adeola O (2014) Evaluation of amino acid and energy utilization in feedstuff for swine and poultry diets. Asian Australas. J. Anim. Sci., 27: 917–925.

Sugiharto S (2022) Feeding fermented agricultural byproducts as a potential approach to reduce carbon footprint from broiler production – a brief overview. Reviews in Agricultural Science, 10: 90–100.

Sugiura K, Yamatani S, Watahara M & Onodera T (2009) Ecofeed: animal feed produced from recycled food waste. Veterinaria Italiana, 45: 397–404.

Toda K, Chiba K & Ono T (2007) Effects of components extracted from okara on the physicochemical properties of soymilk and tofu texture. Journal of Food Science, 72: 108–113.

Genome-Wide Association Analysis of the Changes in Malate Release Under Aluminum Stress in *Arabidopsis thaliana*

Congxiao Wang[1], Masafumi Shimizu[1], Hiroyuki Koyama[1] and Yuriko Kobayashi[1]

[1] Faculty of Applied Biological Sciences, Gifu University, 1-1 Yanagido Gifu 501–1193, Japan

INTRODUCTION

Soil aluminum toxicity, characterized by an excessive presence of soluble aluminum ions in the soil, typically occurs in acidic soils (Shetty,2021). This issue is prevalent on a global scale and poses significant challenges to agriculture and ecosystems. Acidic soils generally exhibit low pH values, primarily due to factors such as atmospheric acid rain, soil erosion, and prolonged use of acidic fertilizers. In acidic soils, aluminum exists in the form of soluble aluminum ions. These aluminum ions severely impact the growth of plant roots. Aluminum toxicity is primarily characterized by damage to root cell walls, inhibition of root growth, and a resulting decrease in a plant's ability to absorb and utilize water and nutrients (Panda, 2009). Soil aluminum toxicity also has repercussions on natural ecosystems (Alengebawy, 2021). It can lead to soil acidification, disrupt the activities of soil microorganisms, and disturb the balance of the soil ecosystem. Addressing the issue of soil aluminum toxicity is crucial for enhancing agricultural sustainability.

Plants employ a variety of physiological, biochemical, and molecular strategies to resist aluminum toxicity (Inostroza-Blancheteau ,2012). Among these strategies, the secretion of organic acids plays a pivotal role, with malate being a key player in this process. The mechanisms of organic acid secretion primarily involve the active efflux mechanism, transporter-mediated organic acid efflux, etc. Through these pathways, malate, secreted by plants, can chelate with aluminum ions in the soil, forming insoluble aluminum-organic acid salts (Rout, 2001). This, in turn, lowers the concentration of free aluminum ions in the soil solution, thereby alleviating the impact of aluminum toxicity on plants.

Genome-Wide Association Analysis (GWAS) is a crucial genetic research method used to investigate the relationships between genes and specific traits or diseases (Visscher,2012). This method aims to discover genetic variations that influence particular traits and how these genetic variations impact an individual's characteristics, susceptibility to diseases, and more. GWAS explores the relationships between hundreds of thousands to millions of genetic markers, such as Single Nucleotide Polymorphisms (SNPs), and an individual's phenotypic expressions. This approach helps us comprehend the intricate connections between genes and traits, as well as how different genotypes affect an individual's response to specific characteristics. Genome-Wide Association Analysis serves as a pivotal tool in modern genetic research, which aids in gaining profound insights into the complex interplay between genes and traits, providing essential information for disease prevention, diagnosis, and treatment. Furthermore, it offers valuable tools for research in fields such as agriculture, ecology, and beyond.

MATERIALS AND METHODS

Arabidopsis Accessions

Plant Materials Seeds of natural *A. thaliana* accessions were obtained from the Arabidopsis Biological Resource Center (Columbus, OH, USA), The Nottingham Arabidopsis Stock Center (Nottingham, UK), and the RIKEN BioResource Center (Tsukuba, Japan). Progeny lines were obtained by controlled self-pollination using the single-seed descent method.

Malate Release and Measurement

Seedlings were grown for 4 d aseptically in the manner of Hoekenga et al. (2003), substituting 100% MGRL solution with 1% (w/v) suc. at pH 5.0. Other conditions were as described above. Seeds were sown on 10-mm squares of plastic mesh (25 plants), after 4 d, the seedlings were transferred to wells in a 6-well microtiter plate containing 2 mL of root exudate collection medium along with the aluminum stress environment (10μM Al, 2% MGRL nutrients, and 1% [w/v] suc.), and gently shaken on a rotary shaker (60 rpm) at 25°C in darkness for 24 hours. Malate concentrations in exudation media were determined by a NAD/NADH cycling-coupled enzymatic method as Takita et al., (1999) or capillary electrophoresis as described (Hoekenga et al., 2003). All experiments were carried out at least three times and means and SE values are reported.

Genome-wide Association study

The GWAS calculations were completed using the GWAPP(http://gwas.gmi.oeaw.ac.at), a web application for GWAS. The genome-wide SNPs used in this study were obtained from a public database (https://cynin.gmi.oeaw.ac.at/, http://1001genomes.org/index.html). In total, 171,474 SNPs were used for the GWAS after SNPs with missing data or a minor allele frequency below 10% were removed. The average r 2 values were plotted against the number of top-ranked SNPs in the GWAS. A local association study was similarly conducted for 80 *A. thaliana* accessions using the TASSEL program with more polymorphisms in the peak region of chromosome 4

(Figure 1A and Supplemental Table 3) identified through sequencing or mined from a public database (http://1001genomes.org/index.html).

RESULTS AND DISCUSSION

The malate releasement over a 24-hour period was measured in 42 accessions under 10 μM aluminum stress. It was observed that there is a significant variation in malic acid secretion among the different accessions, which is favorable for conducting Genome-Wide Association Studies (GWAS). This is further supported by the distinct root lengths of different accessions under aluminum stress, as illustrated in Fig. 2. In general, variations in root length under aluminum stress are indicative of different levels of aluminum tolerance. Longer root lengths suggest less impact from aluminum stress and higher malic acid secretion. Based on these results, it is demonstrated that the selected accessions in this experiment are suitable for further GWAS analysis.

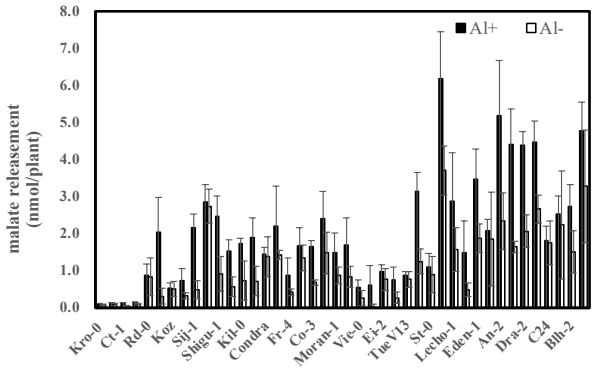

Fig. 1: Malate releasement under 24-hour aluminum stress in 42 Accessions

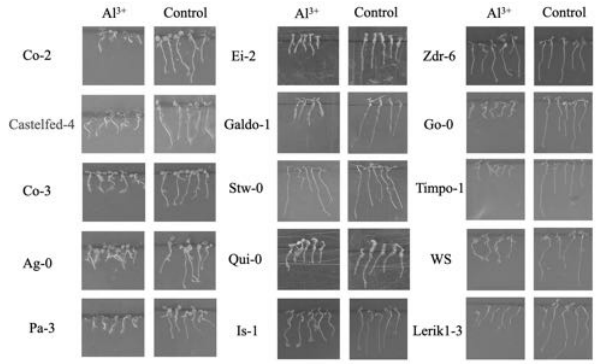

Fig. 2: Different root length under 24-hour aluminum stress

Several candidate genes can be identified through Manhattan plots, with a prominent peak on the third chromosome. As more accessions are included in the measurements, this result becomes increasingly pronounced. After identifying the position of this gene, it can be subjected to further validation and analysis.

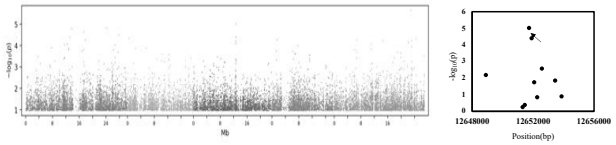

Fig. 3: Manhattan plots from the genome-wide association study (GWAS) of Aluminum tolerance in *A.thaliana*. Figure right side shows the position of a candidate gene.

Due to the number of accessions, the precision of this GWAS is limited. If we continue to measure malate release in different accessions, the results will become more reliable. Based on the results of GWAS, further analysis can be conducted to understand the underlying mechanisms, and validation can be performed by using knockout seeds for the specific gene.

REFERENCES

Shetty R, Vidya CSN, Prakash NB et al. (2021) Aluminum toxicity in plants and its possible mitigation in acid soils by biochar: A review[J]. Science of the Total Environment, 765: 142744.

Panda S K, Baluška F and Matsumoto H. (2009) Aluminum stress signaling in plants. Plant signaling & behavior, 4(7): 592–597.

Alengebawy A, Abdelkhalek ST, Qureshi SR et al. (2021) Heavy metals and pesticides toxicity in agricultural soil and plants: Ecological risks and human health implications. Toxics, 9(3): 42.

Inostroza-Blancheteau C, Rengel Z, Alberdi M et al. (2021) Molecular and physiological strategies to increase aluminum resistance in plants. Molecular Biology Reports, 39: 2069-2079.

Rout G, Samantaray S and Das P. Aluminium toxicity in plants: a review. Agronomie, 2001, 21(1): 3-21.

Visscher PM, Brown MA, McCarthy MI et al. (2012) Five years of GWAS discovery. The American Journal of Human Genetics, 90(1): 7–24.

Hoekenga OA, Vision TJ, Shaff JE et al. (2003) Identification and characterization of aluminum tolerance loci in Arabidopsis (Landsberg erecta x Columbia) by quan- titative trait locus mapping: a physiologically simple but genetically complex trait. Plant Physiol., 132: 936–948.

Takita E, Koyama H and Hara T (1999) Organic acid metabolism in aluminum- phosphate utilizing cells of carrot (Daucus carota L.). Plant Cell Physiol., 40: 489–495.

Alleviative Effect of Gypsum to Rhizotoxic Stressors on Acid Soil

Koffi Pacome Kouame[1], Raj Kishan Agrahari[1], Yasufumi Kobayashi[2], Toshihiro Watanabe[3], Akiko Maruyama[4], Koyama Hiroyuki[1] and Yuriko Kobayashi[1]

[1] The United Graduate School of Agricultural Science, Gifu University, 1-1 Yanagido, Gifu-shi, Gifu 501-1193, Japan
[2] Japan International Research Center for Agricultural Science, 1-1 Owashi, Tsukuba-shi, Ibaraki 305-8686, Japan
[3] Faculty of Agriculture, Hokkaido University, Kita 8, Nishi 5, Kita-ku, Sapporo, Hokkaido 060-0808, Japan
[4] Faculty of Agriculture, Kyushu University, 744 Motooka, Nishi-ku, Fukuoka 819-0395, Japan

INTRODUCTION

This study aimed to elucidate the mechanisms of the alleviative effect of gypsum on Al toxicity using Arabidopsis accessions, with a focus on sulfur (S). In acid soils (pH<5.5), Al^{3+} toxicity and phosphates (Pi) deficiency drastically reduce crop yield worldwide (Kochian et al.,2015). Gypsum improves subsoil acidity by chelating with Al^{3+} to form an aluminum sulfate ($AlSO_4^+$) which is less toxic and increases S and Pi uptake. In fact, when Arabidopsis and crops grow in acid soil, the toxicity could be alleviated by $CaSO_4$ (pH 4.7) as well as $CaCO_3$ (pH 5.5). In the case of Al toxicity, Plants have evolved bi-directional mechanisms of Al tolerance like Al-detoxification (Internal tolerance) and exclusion (external tolerance) to cope with the constraints of Al toxicity in acid soils (Kochian et al.,2015).

Organic acids have been identified in several crops like soybean (*Glycine max*) (Siguira et al.,2021) for citrate and Arabidopsis (Kobayashi et al.,2007) and Wheat (Sasaki et al.,2004) for malate. A new study revealed that organic acid secretion enhances P acquisition by S application (Siguira et al.,2021). Sulfur(S) has been proven to play an important role in regulating plant responses to various biotic and abiotic stress (Sheng et al.,2016). Sulfate deficiency causes growth retardation, decreases Glutathione (GSH), and Glucosinolate (GSL), and reduces crop yields and quality (Sheng et al.,2016). In Arabidopsis, *SULTR3:5* was colocalized with *SULTR2:1* low-affinity sulfate transporter in the xylem parenchyma and pericycle cell root (Kataoka et al., 2004b). Sulfur application mitigated Mn toxicity by sequestering Mn into the vacuole (Sheng et al.,2016).

MATERIALS AND METHODS

Hydroponic culture materials

Arabidopsis (*Arabidopsis thaliana*) accession wild type Columbia Col-0 was obtained from the RIKEN BioResource Center and Al sensitive accessions from Arabidopsis Biological Resource Center Wei-0 (CS22622),Ts-5(CS1558), *SULTR2:1-KO*, *SULTR3:1-KO*, *SULTR3:5-KO* from (Kyushu university).

Soil culture: Soybean and Wheat were used for the soil experiment. First, the soil was supplemented with basal nutrients. Then, we proceeded to the pH measurement and Al exchangeable extraction (Kissel et al., 1971).

Hydroponic culture and root measurement: The seedlings of Arabidopsis were grown hydroponically in 2% strength modified MGRL medium into 10% without Pi as described by Kobayashi et al. (2007). pH was adjusted to 5.0 with $AlCl_3.6H_2O$ (4μM) under a 12-h-light/ 12-h-dark photoperiod (120μmol quanta $m^{-2}s^{-1}$).

Malate measurement: The same accessions used for the hydroponic culture were grown in a liquid medium according to Hoekenga et al. (2003). The basal nutrient solution is composed of 100% MGRL (high strength) with 1% sucrose at pH=5.6. 25 Seeds were sown on each 10mm square plastic mesh in Magenta GA-7 vessels containing 150ml of high-strength media.

RNA extraction and quantitative RT-qPCR: About 120 seeds were sown in basal MGRL solution (2%) plus Pi (Phosphate). After 10d growth, the seedlings were stressed in basal medium (2%) as those used in malate release without sucrose. Total RNA was isolated from the roots according to Suzuki et al. (2003) using Sepasol-RNA I Super G (Nacalai Tesque) following the methods indicated by the manufacturer.

RESULTS and DISCUSSION

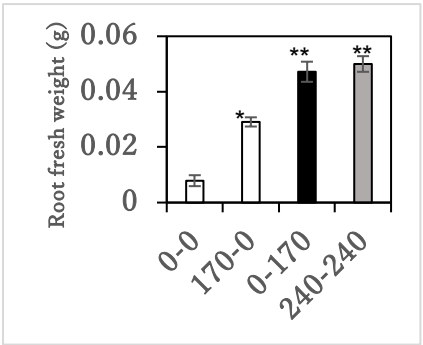

Fig. 1: Fresh weight plotted against different treatments 0-0 indicated soil not treated, 170-0 soil treated with $CaCO_3$, 0-170 soil treated with $CaSO_4$, and 240-240 soil with both treatments.

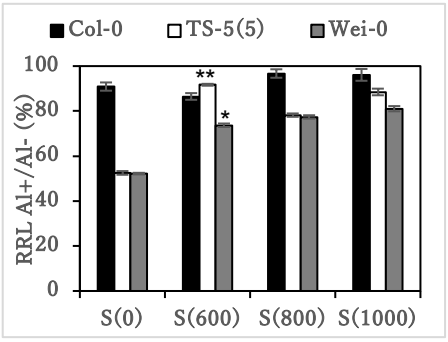

Fig. 2: Relative Root Length plotted against different concentrations of $CaSO_4$. S represents $CaSO_4$ treatment

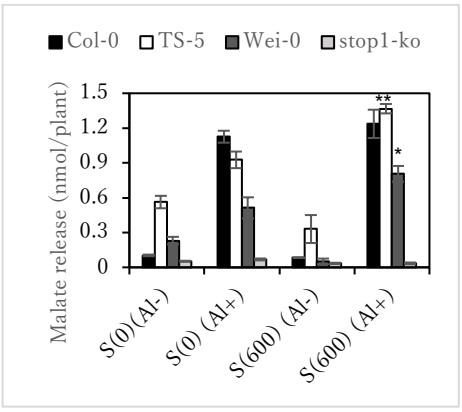

Fig. 3: Malate release. Ts-5 and Wei-0 secreted more malate with CaSO4(600 µM) than when no treatment (control) both in the presence of Al(10µM) 12h later. S means $CaSO_4$ treatment.

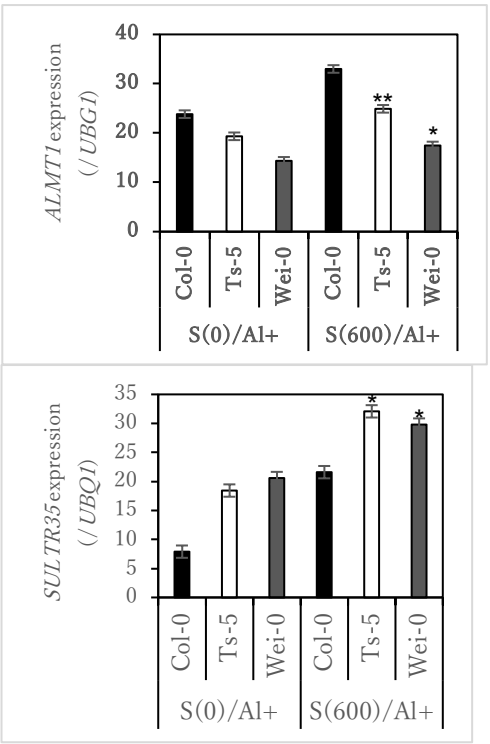

Fig. 4: *AtALMT1* and *SULTR35* expression levels were significantly induced in Ts-5 and Wei-0 with CaSO4(600 µM) then when no treatment (control). In the presence of Al(10µM) 24h later. S means $CaSO_4$ treatment. *AtALMT1* and *SULTR35* could be involved in Al regulation.

Gypsum triggered *AtALMT1* which encodes AtALMT1 proteins to bind with Al. On the other hand, *SULTR35* could be involved in internal and external detoxification during the sulfate transfer from root to shoot.

REFERENCES

Hoekenga OA, Vision TJ, Shaff JE, Monforte AJ, Lee G P, Howell SH and Kochian LV (2003) Identification and characterization of aluminum tolerance loci in Arabidopsis (Landsberg erecta×Columbia) by quantitative trait locus mapping. A physiologically simple but genetically complex trait. Plant Physiology, 132(2): 936–948.

Kataoka T, Hayashi N, Yamaya T and Takahashi H (2004b) Root-to-shoot transport of sulfate in Arabidopsis. Evidence for the role of SULTR3; 5 as a component of low-affinity sulfate transport system in the root vasculature. Plant Physiology, 136(4): 4198–4204.

Kissel DE, Gentzsch EP and Tomas GW (1971) Hydrolysis of nonexchangeable acidity in soils during salt extractions of exchangeable acidity. Soil Sci., 111:293–297.

Kobayashi Y, Hoekenga OA, Itoh H, Nakashima M, Saito S, Shaff JE et al. (2007). Characterization of AtALMT1 expression in aluminum-inducible malate release and its role for rhizotoxic stress tolerance in Arabidopsis. Plant Physiology, *145*(3): 843–852.

Kochian LV, Piñeros MA, Liu J and Magalhaes JV (2015) Plant adaptation to acid soils: the molecular basis for crop aluminum resistance. Annual Review of Plant Biology, 66: 571–598.

Sasaki T, Yamamoto Y, Ezaki B, Katsuhara M et al. (2004) A wheat gene encoding an aluminum-activated malate transporter. The Plant Journal, 37(5): 645–653.

Sheng H, Zeng J, Liu Y, Wang X et al. (2016) Sulfur mediated alleviation of Mn toxicity in polish wheat relates to regulating Mn allocation and improving antioxidant system. Frontiers in Plant Science, 1382.

Sugiura H, Miyaji S, Yamamoto S et al. (2020) Induction of citrate transporter gene expression in soybean roots by sulfur application. Soil Science and Plant Nutrition, 68(5-6): 547–552.

Suzuki Y, Hibino T, Kawazu T, Wada T, Kihara T and Koyama H (2003) Extraction of total RNA from leaves of *Eucalyptus* and other woody and herbaceous plants using sodium isoascorbate. Biotechniques 34: 988–990.

Study on the Effect of Ca-Binding Chemical Agents to Induce Intumescence Injury in Some Tomato Cultivars

Natassia Clara Sita[1,2], Sachiko Ohno[2], Yoshikazu Kiriiwa[2,3] and Katsumi Suzuki[2,3]

[1] The United Graduate School of Agricultural Science, Gifu University, 1-1 Yanagido, Gifu-shi, Gifu 501-1193, Japan
[2] Faculty of Agriculture, Shizuoka University, 836 Ohya, Suruga-ku, Shizuoka 422-8529, Japan
[3] Graduate School of Integrated Science and Technology, Shizuoka University, 836 Ohya, Suruga-ku, Shizuoka 422-8529, Japan

INTRODUCTION

Intumescence injury is a physiological disorder usually found in Japan's greenhouse cultivation. It is characterized by the elongation of epidermal and/or palisade parenchyma cells on the adaxial/abaxial surfaces of leaves or stems (Suzuki et al. 2020). Intumescence injury, also known as oedema or edema, commonly occurs in Solanaceae, such as tomatoes (Atkinson 1893) and potatoes (Douglas 1907).

Environmental conditions, such as low UV irradiance (Lang and Tibbitts 1983) and high humidity (Atkinson 1893; Lang and Tibbitts 1983), are the main factors causing intumescence injury in greenhouse or plant factories. Other studies found that differences in the intumescence severity among several cultivars of tomato were genetically dependent (Prinzenberg et al. 2022). Previous reports suggested that chemical agents could contribute to intumescence injury, such as copper spray in cauliflower (Schrenk 1905) and potato leaves (Douglas 1907).

Recent findings reported that calcium (Ca) deprivation can cause intumescence injury as opposed to other physiological disorders, such as tip burn, blossom end rot (White and Broadley, 2003), and internal browning (Suzuki et al. 2019). Ca is a macronutrient essential for maintaining the structural integrity of cell walls and membranes (Marschner, 1995; White and Broadley, 2003). A lack of Ca can result in intumescence injury in the leaves of Russet Burbank potato (Schabow and Palta 2019) and several tomato cultivars (Sita et al. 2023).

Recent research conducted in our laboratory discovered that the application of ethylene glycol tetraacetic acid (EGTA), a Ca-chelator known to produce tipburn in lettuce (Carassay et al. 2012), caused intumescence injury to occur in cabbage leaves. Ca-chelators (EGTA and EDTA) and Ca-inhibitors (such as $LaCl_3$ and nifedipine) are known to inhibit growth and cause Ca-deficiency-related injuries in vegetables. However, no study has clarified the chemically induced intumescence injury recently.

Thus, this study aimed to identify the correlation and significance of the Ca deficit in tomato leaves caused by Ca-binding chemical treatment. This study also investigated the correlation between Ca nutrient solution and Ca-binding chemical agents to intumescence injury in tomato leaves.

MATERIALS AND METHODS

Experimental conditions—Three cultivars of tomato (*Solanum lycopersicum*): 'Rinka 409', 'Misora 64', and 'CF Momotaro York' were used as plant materials in this study. All plants were sown in rockwool cube (1 × 1 × 1 inch), and after seven days of sowing, seedlings were transferred into an artificial climate chamber and the nutrient solution (Enshi formula nutrient solution ½ strength (EC 1.2 $dS \cdot m^{-1}$, diluted in well-water (EC 0.15 $dS \cdot m^{-1}$), which contained a total of 4.5 $me \cdot L^{-1}$ Ca) were supplied from the bottom with aeration. The average temperature during all experiments was 23.5-25 °C with a relative humidity of 50-78 %.

Experiment 1 and 2—The topical treatments used in Experiment 1 were EGTA and $LaCl_3$, each 1 mM and 10 mM, and distilled water (control). All treatments were applied on the leaves' edges on the adaxial and abaxial surfaces. Treatments were applied once three weeks after sowing on the third leaves, and intumescence injury severity was observed one week after treatment.

The topical treatments used in Experiment 2 were EDTA, EGTA, $LaCl_3$, nifedipine, each 10 mM, and control. All treatments were applied on the second leaves' whole adaxial and abaxial surfaces. Treatments were applied thrice weekly, and the intumescence injury severity was observed afterward.

Experiment 3—Three levels of Ca nutrient solution were used, each containing 0.5 $me \cdot L^{-1}$ Ca, 4.5 $me \cdot L^{-1}$ Ca, and 9.5 $me \cdot L^{-1}$ Ca. In this experiment, four topical treatments, including control, EGTA 10 mM, $LaCl_3$ 10 mM, and nifedipine 10 mM, were applied four times as in Experiment 2. The intumescence injury severity was scored after ten days of treatment.

Intumescence injury severity scoring—The following scale determined intumescence injury severity: 0 = no intumescence, 1 = intumescence slightly appeared, 2 = moderate intumescence, 3 = severe intumescence, 4 = severe intumescence with slightly to moderate wilting, 5 = severe intumescence with sever wilting.

Statistical analysis—Student's t-test was used to identify the differences between control and Ca-binding chemical treatments in each experiment.

RESULTS AND DISCUSSION

Experiments 1 and 2 showed that multiple applications of Ca-binding agents are more effective than one-time applications to chemically induced intumescence injury. In Experiment 1, Ca-binding agents did not significantly induce intumescence in 'Rinka 409', while in Experiment 2, only nifedipine 10 mM significantly induced intumescence (data not shown). Significant differences between control and Ca-binding chemical agents were observed in 'Misora 64' leaves in Experiment 2 (Fig 1). Among all treatments, only EDTA did not significantly induce intumescence injury.

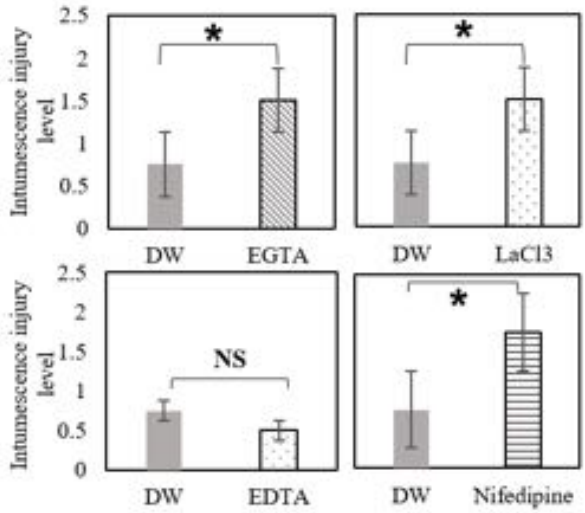

Fig. 1: Effect of several Ca-binding chemical agents (each 10 mM) to intumescence injury on 'Misora 64' leaves. (* indicate significant difference at $p < 0.05$ by Student t-Test, NS, not significant).

Experiment 3 showed a negative correlation between Ca concentrations in nutrient solution and intumescence injury severity in 'Misora 64' (Fig 3). This was aligned with the previous report, which suggested that increasing Ca concentration in nutrient solution could lower the degree of intumescence injury (Sita et al. 2023). However, Nifedipine 10 mM, although not significant, induced intumescence injury even in 9.5 me·L^{-1} Ca concentration, indicating that Ca-binding chemical agents could induce intumescence injury in tomato leaves.

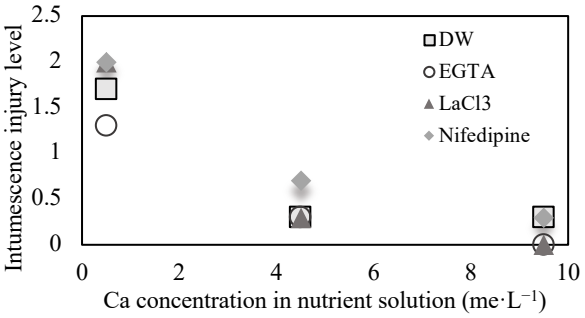

Fig. 2: Correlation between Ca concentration in nutrient solution and intumescence injury level on 'Misora 64' leaves with Ca-binding chemical treatments applied. (DW= distilled water, each Ca-binding agent concentrated 10 mM).

Previous studies showed that 'CF Momotaro York' showed tolerance against intumescence injury, even when conditioned in low UV and high relative humidity environments and when the Ca was insufficient in nutrient solution (Sita et al. 2023). We treated this cultivar with Ca-binding agents to chemically induce intumescence in this study. The result, however, showed no intumescence occurrence in all experiments, indicating other factors might contribute to the tolerance trait of this cultivar, such as genetic factors (Prinzenberg et al. 2022) or the differences related to its morphological characteristics. Further studies are needed to clarify this phenomenon.

This study concluded that EGTA, $LaCl_3$, and nifedipine induced intumescence injury in 'Misora 64' and 'Rinka 409'. Ca-binding chemical agents could induce intumescence injury in 'Misora 64' and 'Rinka 409', even under insufficient Ca conditions.

REFERENCES

Atkinson GF (1893) Oedema of the tomato. Cornell Univ. Agr. Stn. Bull., 53: 77–108.

Carassay LR, Bustos DA, Golberg AD, Taleisnik E (2012) Tipburn in salt-affected lettuce (*Lactuca sativa* L.) plants results from local oxidative stress. J. Plant Physiol., 169: 286–293.

Douglas GE (1907) The formation of intumescences on potato plants. Botanical Gazette, 43: 233–250.

Lang SP and Tibbitts TW (1983) Factors controlling intumescence development on tomato plants. J. Amr. Soc. Hort. Sci., 108: 93–98.

Marschner H (1995) Mineral nutrition of higher plants, 2nd ed. Academic Press, London.

Prinzenberg AE, van der Schoot H, Visser RGF, Marcelis LFM, Heuvelink E and Schouten HJ (2022) Both major QTL and plastid-based inheritance of intumescence in diverse tomato (*Solanum lycopersicum*) RIL populations under different light conditions. Plant Breed., 141: 574–584.

Schabow JE and Palta JP (2019) Intumescence injury in the leaves of russet burbank potato plants is mitigated by calcium nutrition. Am. J. Potato Res., 96: 6–12.

Schrenk Hv (1905) Intumescences formed as a result of chemical stimulation. Missouri Botanical Garden Annual Report, 1905: 125–148.

Sita NC, Kousaka A, Tamoi R, Ozawa C, Iriawati, Kiriiwa Y and Suzuki K (2023) Incidence of intumescence injury in several tomato cultivars under different calcium conditions. Hort. J. Preview., doi: 10.2503/hortj.QH-072.

Suzuki K, Ozawa C and Kiriiwa Y (2020) Morphological study on the incidence of intumescence injury in tomato plant leaves. Hort. J., 89: 567–574.

Suzuki K, Suzuki D, Numajiri M, Matsushiro J, Yamane M and Y. Kiriiwa (2019) Anatomical analysis of internally brown tomato fruit. Hort. J., 88: 263–269.

White PJ and Broadley MR (2003) Calcium in plants. Ann. Bot., 92: 487–511.

Effect of Plastic Mulch Residues on Plant Growth and Soil Properties

Shiamita Kusuma Dewi[1], Zaw Min Han[2], Yongfen Wei[3] and Fusheng Li[3]

[1]The United Graduate School of Agricultural Science, 1-1 Yanagido, Gifu-shi, Gifu 501-1193 Japan
[2]Faculty of Engineering, Gifu University, 1-1 Yanagido, Gifu-shi, Gifu 501-1193 Japan
[3]River Basin Research Center, Gifu University, J1-1 Yanagido, Gifu-shi, Gifu 501-1193 Japan

INTRODUCTION

Mulching is a common practice used by farmers to modify soil temperature, minimize weed competition, reduce soil erosion and evaporation, and improve soil physical condition. However, due to its low recycling rates, conventional plastic mulch (polyethylene (PE) plastic mulch) tends to accumulate in the soil after use, potentially harming soil quality and reducing crop yield.

Biodegradable mulch is becoming increasingly favored as an eco-friendly substitute for PE plastic mulch, given its capacity to completely break down in the soil, making it more environmentally friendly. While biodegradable mulch film is designed to decompose within two years, its degradation process is influenced by environmental factors such as temperature, moisture content, and the microbial community present in the soil. Furthermore, biodegradable film degrades more rapidly than PE films. Thereby causing a greater impact on agricultural land and crops (Zhou et al., 2023).

On the other hand, during agricultural practice, adding soil amendments of organic materials such as crop residues, compost, and animal manure can increase soil fertility, improve soil properties, and enhance microbial activities. However, the effect of soil amendments on plastic mulch residues contaminated soil remains unknown. To study the effect of plastic mulch residues on plant growth and soil properties, as well as the changes in this impact under the addition of soil amendments, a pot experiment is designed and carried out.

MATERIALS AND METHODS

Soil sample and amendments – Soil sample was collected from vegetable fields located in Gifu University. Two soil amendments were used in the study: compost and biochar. Compost was made from a mixture of food waste and cow manure. The biochar was derived from rice husk and was obtained from the TAKII SEED corporation. The soil was sieved through a 2-mm mesh sieve and homogenized.

Mulch Plastic – Low-density polyethylene (PE) and Polybutylene succinate adipate mulch films (Biodegradation, here referred to as Bio) were manually cut into a square shape with a cutter and ruler. The size was 10 mm.

Mulch plastic and amendments addition to soil – The soil sample was mixed with each type of mulch plastic film at a concentration of 0.1% (w/w dry weight of soil) and soil amendment with a dose of 0.75% (w/w dry weight of soil). Therefore, 0.5 g of each mulch plastic film and 3.75 g of each soil amendment were mixed into 500 g of soil by stirring with a spoon in a big container before transferring the mixture into the pot. The potted experiment design and treatments are shown in **Fig. 1**. Each treatment has 3 replicates; therefore, a total of 27 pots were prepared.

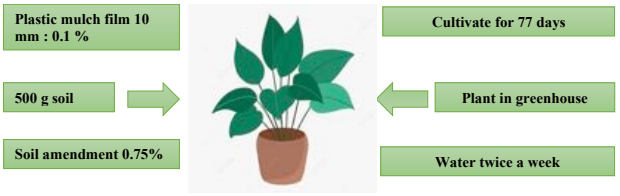

Fig.1: Design of the potting experiment

Table 1. Properties of soil and soil amendment

Parameter	Soil	Compost	Biochar
pH	6.33 ± 0.00	8.08 ± 0.05	10.09 ± 0.04
EC (dS m^{-1})	1.48 ± 0.08	6.25 ± 0.17	1.01 ± 0.01
OM content (%)	10.62 ± 0.52	67.83 ± 2.61	17.03 ± 4.31
TN (mg g^{-1})	5.81 ± 3.20	33.39 ± 0.52	5.10 ± 0.97
TP (mg g^{-1})	1.31 ± 0.05	1.30 ± 0.09	0.74 ± 0.04
TK (mg g^{-1})	8.34 ± 0.16	4.95 ± 1.60	ND
$N\text{-}NO_2^-$ (mg g^{-1})	0.01 ± 0.00	0.04 ± 0.00	0.01 ± 0.00
$N\text{-}NO_3^-$(mg g^{-1})	ND	0.05 ± 0.03	0.01 ± 0.00
EK (mg g^{-1})	7.61 ± 0.48	4.02 ± 0.16	ND

Note: Values represent mean ± standard deviation (n = 3). EC: electrical conductivity; OM: organic matter; TN: total nitrogen; TP: total phosphorous; TK: total potassium; $N\text{-}NO_2^-$: water-soluble nitrite; $N\text{-}NO_3^-$: water-soluble nitrate; EK: Exchangeable potassium.

The pH and electrical conductivity (EC) of the supernatant suspension were determined using a 1:5 (w/v) ratio of sample to water. The organic matter (OM) content was determined as the incineration loss at 600º. Total nitrogen (N) in soil and plant tissues was analyzed by CN analyzer. The alkaline potassium persulfate digestion-UV spectrophotometer method measured soil and plant tissues' total phosphorus (P). 1 mol L^{-1} hot HNO_3 extraction method was used to determine total potassium (K) in soil and plant. Exchangeable-K of soil was extracted with 1 M ammonium acetate, water-soluble nutrient extracted with 1:5 = soil: ultrapure water and

measured with ion chromatograph method. Soil dehydrogenase activity was measured using triphenyl tetrazolium chloride (TTC). The soil and soil amendments used in this study are summarized in **Table 1**.

Statistical analysis – Statistical analyses were conducted using SPSS 19.0 ($p \leq 0.05$). Analysis of variance (ANOVA) – two ways were used to determine the differences between different treatments. Tukey's multiple comparison tests method at the probability level 0.05 was used to separate mean differences of the plant growth performance and soil properties.

RESULTS AND DISCUSSION

Plant growth characteristics — Two-way ANOVA result (**Table 2**) revealed that plastic type significantly affected the total nitrogen and magnesium uptake. On the contrary, all plant morphological traits were not significantly affected by plastic type. The soil amendments effect was significant for total dry weight and total nitrogen uptake. The interaction effect (plastic type x soil amendment) was not significant for all plant growth characteristics.

Table 2: Two-way ANOVA results: significance (*p*-value) of the independent variables plastic-type, soil amendments, and interaction effects on plant growth characteristics

Plant growth characteristics	*p* value		
	Plastic type	Soil amendment	Plastic type x soil amendment
SDW	0.078	0.018	0.799
RDW	0.204	0.068	0.292
TDW	0.096	0.025	0.558
SL	0.683	0.097	0.394
LA	0.869	0.322	0.571
LN	0.402	0.126	0.513
R/S	0.487	0.144	0.279
TNU	0.006	0.014	0.065
TPU	0.681	0.695	0.709
TMg	0.026	0.289	0.432

Note: TNU: Total nitrogen uptake (mg g -1); TPU: Total phosphorus uptake (mg g -1); TMg uptake: Total magnesium uptake (mg g -1); SL: stem length (cm); LA: leaf area (cm2); LN: leaves number (leaves); SDW: Shoot dry weight (g); RDW: Root dry weight (g); TDW: Total dry weight (g). The effect was significant for *p-value* < 0.05.

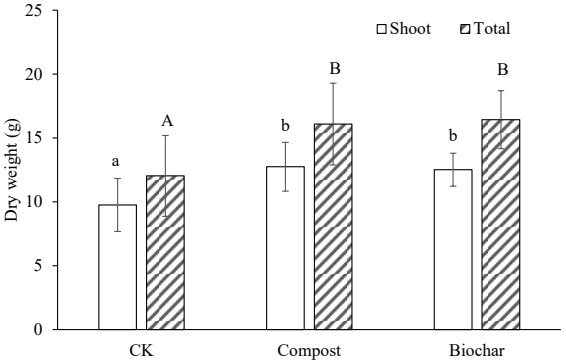

Fig 2: Effect of soil amendments on the dry weight of plants in all treatments. Different lowercase letters indicate significant differences between treatments ($P < 0.05$).

In **Fig 2**, it is demonstrated that the addition of compost and biochar led to a significant increase in both shoot and total dry weight, indicating a positive effect on plant growth.

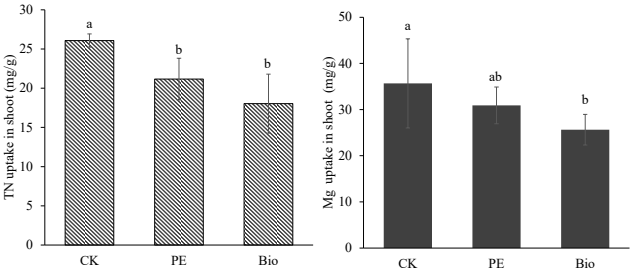

Fig 3: Effect of plastic mulch residues on the total nitrogen and total magnesium uptake of plants in all treatments. Different lowercase letters indicate significant differences between treatments ($P < 0.05$).

As shown in **Fig 3**, the effects of plastic mulch residues and soil amendments on plant nutrient uptake were examined. The total nitrogen (TN) content in shoots of Japanese mustard spinach shoots grown in pots was significantly decreased by 14.85% and 25.75% in PE and Bio-contaminated soil compared to control, respectively ($p < 0.05$). For magnesium uptake, the presence of PBSA mulch film residues significantly reduced by 28.14% compared to the control treatment.

Soil properties — The results of the two-way ANOVA (**Table 3**) indicated a significant influence of plastic type on dissolved phosphate ($P\text{-}PO_4^-$) levels and soil dehydrogenase activity (DHA). The interaction effect (plastic type x soil amendment) was significant only for soil DHA.

Table 3: Two-way ANOVA results: significance (*p*-value) of the independent variables plastic-type, soil amendments, and interaction effects on soil properties

Soil properties	*p* value		
	Plastic type	Soil amendment	Plastic type x soil amendment
EC	0.256	0.455	0.238
OM	0.834	0.211	0.977
TN	0.82	0.175	0.319
TP	0.758	0.195	0.717
TK	0.961	0.62	0.874
Tca	0.555	0.596	0.694
$N\text{-}NO_2^-$	0.27	0.094	0.615
$P\text{-}PO4^-$	0.035	0.095	0.284
Na^+	0.14	0.258	0.138
DHA	<0.001	0.001	0.026

Note: Na^+: natrium ion. The effect was significant for *p-value* < 0.05.

In this study, the following results were obtained.

1. The presence of plastic mulch film residues significantly decreased TN and TMg uptake.
2. The addition of compost and biochar resulted in a significant increase in both shoot and dry weight.
3. The interaction between plastic-type and soil amendment was found to be significant only in relation to soil DHA.

Comparison of Viral Infection Status of Roses in Japan and Its Effect to Plant Growth

Thiara Celine Suarez[1], Kunio Yamada[2], Takashi Nakatsuka[3] and Masaki Ochiai[2]

[1] The United Graduate School of Agricultural Science, Gifu University, 1-1 Yanagido, Gifu 501-1193, Japan
[2] Faculty of Applied Biological Science, Gifu University, 1-1 Yanagido, Gifu 501-1193, Japan
[3] Faculty of Agriculture, Shizuoka University, 836 Ohya, Suruga-ku, Shizuoka 422-8529, Japan

INTRODUCTION

Roses are considered as one of the popular flowers worldwide for their ecological and cultural significance. In Japan, they are used for medicinal, perfumery and ornamental purposes. As mentioned by the Ministry of Agriculture, Forestry and Fisheries of Japan (2023), the production of roses in the country is among the third largest in terms of cut flower production. However, roses, like all living organisms, are susceptible to various pathogens, pests and diseases like aphids, spider mites and rose mosaic disease (RMD). When this happens, roses suffer from reduction of flower quality, productivity, and plant vigor.

RMD is caused by more than one pathogen including Apple mosaic virus (ApMV) and Prunus necrotic ringspot virus (PNRSV). According to Karlik et al. (2020), the virus is transmitted when virus-infected roses are subjected to grafting onto uninfected plant materials. It was mentioned that empirical evidence suggests that the spread of rose mosaic can occur through root grafts. Infected roses may show no symptoms until after transplanting, and the virus usually persists for the plant's lifetime. Virus infection results in a range of leaf symptoms, including yellow, white, or brownish lines, bands, rings, vein clearing, yellowing, oak-leaf patterns, or blotches. In some cases, only a portion of the plant is impacted.

Research conducted across various parts of the world has shed light on the prevalence of these viral pathogens, contributing to our understanding of the global landscape of RMD.

In Turkey, a comprehensive investigation was conducted, involving the collection of rose samples from diverse regions. These samples underwent testing to identify the presence of distinct viruses that afflict rose plants. The study revealed the presence of PNRSV, rose cryptic virus-1 (RCV-1), rose spring dwarf-associated virus (RSDaV), rose yellow vein virus (RYVV), and ApMV infections (Karanfil, 2021).

Meanwhile, in New Zealand, Milleza et al. (2013) uncovered a similar viral panorama affecting roses. RCV-1, PNRSV, RSDaV, RYVV, and Arabis mosaic virus (ArMV) were identified as the viral agents responsible for infecting roses in this region.

Further investigations by Chen et al. (2022) in Taiwan revealed that a substantial proportion of rose samples - specifically, fifty out of 294 - were affected by a variety of viruses associated with RMD. This study identified a total of ten different viruses contributing to the disease.

In Jordan, Mansour (2010) utilized serological testing via DAS-ELISA to determine the causal agents of RMD. It was determined that this condition could be linked to the presence of PNRSV and ApMV, either as singular infections or in the form of mixed infections.

A study of virus infection was conducted in Japan by Takenaga (2021) wherein it was found that roses were infected with RCV-1 and RSDaV. However, the study was limited to Gifu World Rose Garden and Gifu University Research Field. The inherent constraints of this localized study have emphasized the necessity for a broader, more comprehensive examination of the viral landscape impacting roses across Japan. The pressing knowledge gaps include a scarcity of data concerning the precise viral strains responsible for infecting roses, an in-depth understanding of the physiological damage induced by these viral agents, and the geographic distribution of these infections within the country.

Therefore, the objective of this study is to detect virus from roses planted in rose gardens around Japan and compare the growth and rooting characteristics between virus-infected and non-infected roses. Through this comprehensive approach, it aims to gain a thorough understanding of the complex interplay between viral infections and rose development.

It is with high hopes that results of this study will improve rose cultivation by addressing viral infections, employ a unique approach by comprehensively studying infections and growth effect and envision a future where roses thrive without viral threats.

METHODS

This study consists of two primary experiments designed to investigate the status of viral infections in roses. These experiments aim to provide a comprehensive understanding of the viral infections affecting these plants and their associated effects.

The first experiment involved the systematic collection of rose samples from diverse geographical locations in Japan. These samples will be subjected to identification process using advanced molecular techniques to detect and categorize the specific viral strains affecting the rose samples.

The second experiment will be conducted to evaluate the impact of viral infections on rose plants. In this experiment, both infected and non-infected rose samples

will be examined. The evaluation will include several components. The morphological characteristics of the rose samples will be examined for any visible signs of disease under the microscope. Biochemical analysis of the infected and non-infected samples will be performed to gain insights into the biochemical changes associated with viral infections. This analysis will reveal alterations in the composition of plant tissues and the presence of specific biomarkers linked to viral infections. The effects of viral infections on root and overall growth development will be understood through an investigation of root systems for signs of damage or restricted growth and an assessment of the overall growth patterns of infected versus non-infected roses.

RESULTS AND DISCUSSION

The preliminary collection of samples took place in two key areas: Nishiyama Park in Toyota City, Aichi Prefecture, and Rose Hill Park in Shimada City, Shizuoka Prefecture. Subsequently, an initial examination was conducted to identify any potential symptoms indicating the presence of a virus.

In Nishiyama Park, out of the fifty samples assessed, twenty samples displayed a single symptom. This category was characterized by a variety of specific symptoms, with the most prevalent being moderate to severe chlorotic line patterns observed in six samples. Additionally, there were six samples that exhibited mottling, five with vein banding and netting, one with yellowing on the leaf edge, one with distortion, and one displaying ringspot symptoms. Furthermore, the study identified seventeen samples with mixed symptoms, reflecting a more complex manifestation of leaf issues. These mixed symptoms were combinations of different specific symptoms, such as mosaic, mottling, leaf cutter bee damage, vein banding, yellowing on the leaf edge, distortion, holes in the leaf, and black veins. On the other hand, thirteen samples out of the total did not display any visible symptoms and were categorized as asymptomatic.

In Rose Hill Park Shimada, a total of fifty samples were examined. Among the seventeen samples displaying single symptoms, specific leaf issues were observed. These single symptoms included moderate to severe chlorotic line patterns in three samples, mottling in seven samples, vein banding and netting in five samples, ringspot in one sample, and distortion in one sample. Most of the samples, a total of twenty-seven, exhibited mixed symptoms, which indicated more complex manifestations of leaf issues. The mixed symptoms included combinations like mottling with ringspot, vein banding with ringspot, chlorotic line patterns with ringspot, vein banding with mottling, and others. Six samples were asymptomatic or showed no visible symptoms.

There is a noticeable diversity of symptoms in both locations, encompassing issues like chlorotic line patterns, mottling, vein banding, and ringspot. This diversity suggests that the plant populations in these areas may be experiencing a range of problems, potentially caused by several factors, such as viruses, pests, or environmental stressors. On the other hand, single symptoms might be linked to specific issues, while mixed symptoms might indicate a more complex manifestation of leaf problems. The existence of mixed symptoms in both areas implies that the plant health issues might be complex, involving a combination of factors that contribute to the observed symptoms. The asymptomatic samples suggest that a portion of the plants may be healthy or resilient to the issues observed in other samples.

In summary, these results offer an initial indication into the state of roses in Nishiyama Park and Rose Hill Park Shimada. However, they do not provide a definitive explanation for the observed symptoms. Further research will be conducted.

REFERENCES

Chen TC, Lin YC, Lin CC, Lin YX and Chen YK (2022) Rose Virome Analysis and Identification of a Novel Ilarvirus in Taiwan. Viruses, 14(11): 2537.

Karanfil A (2021) Prevalence and Molecular Characterization of Turkish Isolates of the Rose Viruses. Crop Protection, 143: 2.

Karlik JF, Golino DA, Al Rwahnih M (2020) UC IPM Pest Notes: Roses: Diseases and Disorders. University of California Agriculture and Natural Resources Publication 7463.

Mansour A (2010) Identification of Rose Viruses Associated with Rose Mosaic Disease in Jordan. Jordan Journal of Agricultural Sciences (The University of Jordan). 2: 4.

Milleza, EJM, Ward LI, Delmiglio C, Tang JZ, Veerakone S, Perez-Egusquiza Z (2013) A survey of viruses infecting Rosa spp. in New Zealand. Australasian Plant Pathol., 42: 313–320.

Ministry of Agriculture, Forestry and Fisheries (2023) Statistics of Agriculture, Forestry and Fisheries. Planted area and shipment number of flowers produced in 2022. (In Japanese translated to English) 農林水産統計 令和４年産花きの作付（収穫）面積及び出荷量.
https://www.maff.go.jp/j/tokei/kouhyou/sakumotu/sakkyou_kaki/attach/pdf/index-1.pdf

Takenaga Y (2021) Survey on virus infection in roses. Master Thesis, Gifu University. (In Japanese translated to English) 武永有利 (2021) バラにおけるウイルス感染の実態調査. 修士論文, 岐阜大学大学院自然科学技術研究科.

Reduction of Antibiotic Resistance Genes in Large-Scale Johkasou Treating Residential Area Wastewater

Su Haoning[1], Okumura Shinya [1] and Li Fusheng[2]

[1] Graduate School of Engineering, Gifu University, 1-1 Yanagido, Gifu-shi, Gifu 501-1193, Japan
[2] River Basin Research Center, Gifu University, 1-1 Yanagido, Gifu-shi, Gifu 501-1193, Japan

INTRODUCTION

Antibiotic resistance genes (ARGs) are emerging environmental contaminants and pose serious threat to public health. Wastewater from livestock, agriculture, industry, hospitals, antibiotic manufacturers, and households is the main source of ARGs. For Johkasou, a facility treating household wastewater, the fate and behavior of ARGs remains unclear. In this study, quantitative and qualitative changes of ARGs in the treatment processes of Johkasou was evaluated and the existing state of ARGs in relation to the size of suspended solids in wastewater and sludge was clarified.

MATERIALS AND METHODS

(1) Sample collection and pre-treatment

Water and sludge samples were collected from eight sampling points (**Fig. 1**) in a large-scale Johkasou located in Aichi, Japan. Sampling was performed weekly in 2 months, corresponding to the operation time after cleaning accumulated sludge.

To classify ARGs on suspended solids remaining in water and in sludge, Sample filtration was conducted using sieves with the opening of 250, 125, 75 and 25μm respectively, and a membrane filter with the pore size of 3 μm. The filtrates were used for ARGs quantitation

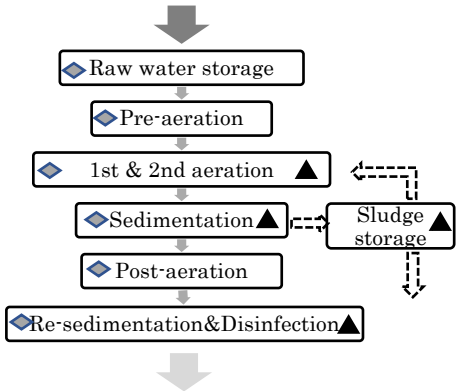

Fig. 1: Flow diagram of the *Johkasou* and sampling points (◇ Water sample ▲ Sludge sample)

(2) DNA extraction and determination of genes

DNA extraction for all samples was conducted using Power Soil DNA Extraction Kit (MOBIO, USA) based on manufacturer's manual. The extracted DNA was stored at −25 °C for determination of target genes by quantitative PCR (qPCR). Two tetracycline resistance gene (*tetG*, *tetM*), two sulfonamide resistance genes (*sul1*, *sul2*), a mobile genetic element (MGE) (integrase class 1 gene, intl 1), and total bacteria reflected by 16S rDNA were quantified by qPCR with the utilization of SYBR® Premix Ex Taq™ (TaKaRa, Japan) based on the manufacturers' manual.

(3) Statistical analysis

Non-metric multidimensional scaling (NMDS) and principal coordinates analyses (PCoA) were created based on the data set comprising the relative amounts of ARGs. These analyses were conducted using the Bray–Curtis distance and implemented through R software.

RESULTS AND DISCUSSION

(1) Fates of ARGs undergoing treatment processes

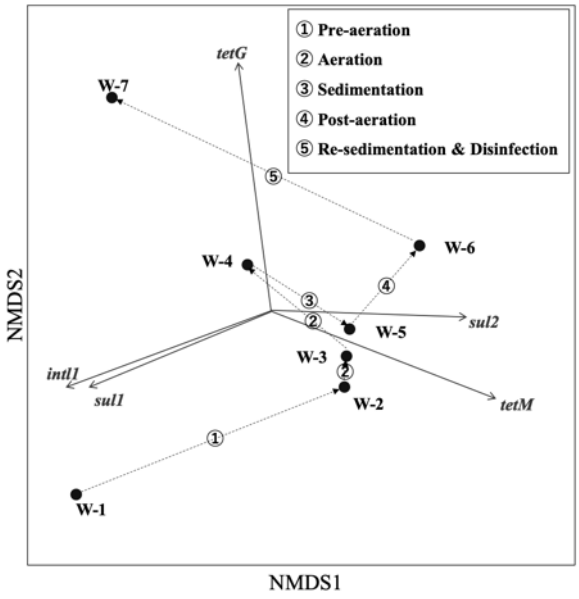

Fig. 2: NMDS biplots of relative ARGs and MGE abundances by target genes (tetG, tetM, sul1, sul2 and intl1) across the treatment process. The process trajectory is represented by dashed lines (in black); original explanatory variables are displayed as vectors (in red).

As shown in **Fig. 2**, The relative amount of ARGs increased during the biological treatment processes (Pre-aeration, 1st aeration and 2nd aeration) and decreased via sedimentation. The Bray-Curtis distance was longest between the biological and sedimentation processes. These results indicate the largest shifts in ARGs occurrence patterns during those processes. Changes in

directions showing the trajectory of sampled sites indicate significant shifts in the ARGs community as a result of having undergone various treatment processes in Johkasou. In the operation of 7 to 63 days after sludge cleaning, the fate and behavior of ARGs were similar, but the extent of ARGs reduction was higher for the time of 28 days from the influent to the effluent (**Fig. 3**)

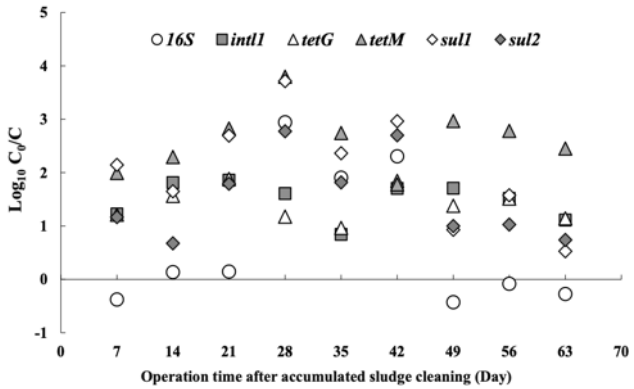

Fig. 3 Log reduction of 16S rDNA, *intl1*, *tetG*, *tetM*, *sul1* and *sul2* during operation of 7 to 63 days after

(2) Fates of ARGs undergoing treatment processes

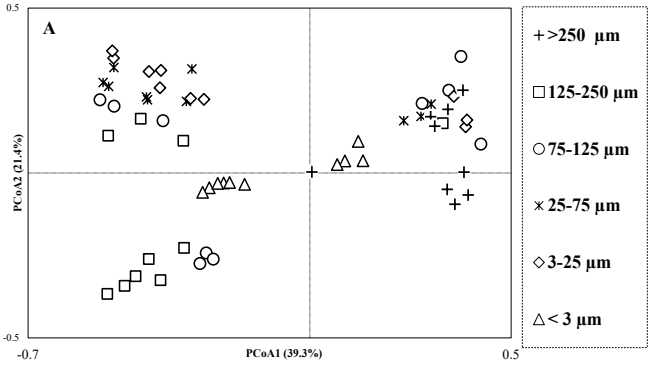

Fig. 4: Bray-Curtis distance-based PCoA of size-fractionated ARGs and MGEs (relative abundances), 'Size fraction' and 'treatment unit' were set as the two

In general, the PCoA results are used to show the distribution of different size related ARGs during the whole treatment process. The PCoA based on the relative abundances of ARGs showed the varied distribution on the suspended solids with different size in wastewater and sludge samples (Fig. 4). The samples with size lower than 3µm clustered together, while there was a shift in genes abundance for the treatment processes from influent and aeration to post-aeration, effluent and sludge. The samples with relative bigger size (25 - 250µm) forming two clusters were not similar while the relative longer distances created by sampling sites. The distances between pre-aeration, sedimentation, post-aeration, settled and re-settled sludge samples with size range of 3 – 25µm were closer, creating another cluster. The results indicated that the fates of ARGs and MGEs were potentially different for different size fractions and treatment process.

Mass fluxes (10^{13}copies/d)	Genes in input	Genes in sludge	Changes of genes during treatment	Genes in output
16S rDNA	3030.5	1983.3	-1016.0	31.2
tetG	58.3	111.3	55.4	2.3
tetM	172.7	1.3	-170.9	0.4
sul1	204.9	468.2	279.0	15.7
sul2	152.6	31.6	-105.0	16.0
intl1	173.3	214.8	46.3	4.9
Total ARGs	588.5	612.5	58.5	34.5

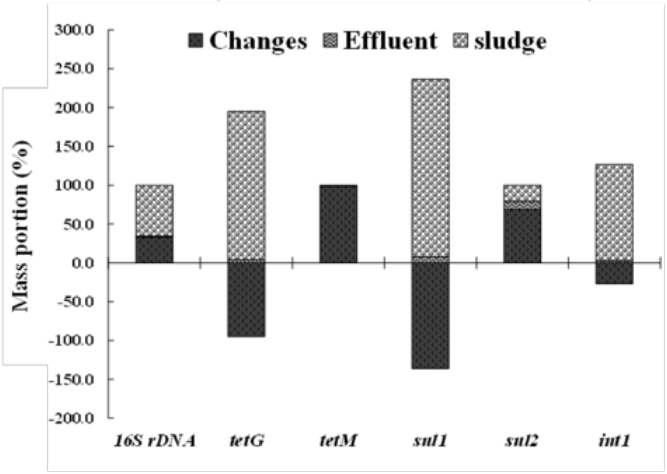

The budget of genes 'mass and distributions in water

Fig. 5: Average mass fluxes of targeted genes of input, sludge, changes and output (upper). Daily mass in percentage of targeted genes (lower).

and sludge are estimated to further evaluate the operative removal process in the Johkasou, and the results were summarized in **Fig. 5**. All the genes demonstrated a relatively high mass flow in biological treatment and sludge. *tetG*, *sul1* and *intl1* behaved similarly in terms of distribution in wastewater and sludge, as well as the negative loss due to biological treatment that means the proliferation of genes. In addition, a significant portion of genes are enriched in the sludge. Although the sludge is periodically removed, during its maximum retention period of two months, a considerable portion will re-enter the aeration unit through backflow. Consistent with results mentioned before, there is a risk that suspended matter, in which small particles have poor settleability, will carry more resistant genes back into circulation or remain in the supernatant and be discharged with the treated water.

Overall, the results improve the understandings on fate and transport of ARGs in household wastewater treatment facility. ARGs carried by suspended solids with small size may be the bottleneck of controlling the spread of ARGs from the hotspots into the receiving environment.

REFERENCES

Yu K, Li P, He Y, Zhang B, Chen Y and Yang J (2020) Unveiling dynamics of size-dependent antibiotic resistome associated with microbial communities in full-scale wastewater treatment plants. Water Res., 187: 116450.

Fate and Behavior of Antibiotic Resistance Genes in Activated Carbon Adsorption

Sri Anggreini[1], Alma Rizky Aurellya[2] and Fusheng Li[1,3]

[1] Graduate School of Engineering, Gifu University, 1-1 Yanagido, Gifu-shi, Gifu 501-1193, Japan
[2] Graduate School of Natural Science and Technology, Gifu University, 1-1 Yanagido, Gifu-shi, Gifu 501-1193, Japan
[3] River Basin Research Center, Gifu University, 1-1 Yanagido, Gifu-shi, Gifu 501-1193, Japan

INTRODUCTION

The dissemination of antibiotic resistance genes (ARGs) in aquatic environments has become a global health issue. Nowadays, antibiotic resistance causes 700,000 deaths globally each year (Mao et al., 2014). Extracellular ARGs (eARGs) in water, such as plasmid or chromosomal DNA, have gained interest due to their durability and contribution to the spread of antibiotic resistance. It has been found that eARGs can persist for several months in water and spread more easily in the aquatic environment compared to intracellular ARGs (iARGs) (Mao et al., 2014).

Powdered activated carbon (AC) is commonly added at the receiving well of water treatment before the coagulation process to enhance organic matter removal. This process produces sludge, which is commonly dewatered. The water is recycled as raw water, while the solid materials containing AC are discharged into the environment. Depending on the physicochemical features of AC, eARGs may penetrate into AC pores before the coagulation process. Further, eARG can probably be carried with solid materials into the environment or carried with recycled water as raw water. eARGs may persist over many generations and enable the dissemination of antibiotic resistance traits via transfer. In this study, the fate and behavior of eARGs during contact with AC were investigated. For this purpose, plasmid pUC19 that carries an ampicillin resistance gene (amp^R) was selected, and ten types of commercially available ACs with different pore size distributions were used.

MATERIALS AND METHODS

Activated carbon—Ten commercially available ACs with different pore size distributions were used, namely carbon A, B, C, D, E, F, G, H, I, and J. Carbon A, B, C, D, and E are coal-based ACs, while carbon F, G, H, I, and J are wood-based ones. All ACs are steam-activated.

Preparation of plasmid-encoded ARGs— Plasmids were propagated by transformation into *E. coli DH5α.* One hundred µL of *E. coli DH5α* were mixed with 10 µL of plasmid. The mixture was incubated on ice for 30 min, then immediately transferred into an incubator at 42 °C for 45 s and placed back on ice for 2 min. After heat shock, the mixture was added into 890 µL of SOC medium and cultured in a shaking incubator (200 rpm) at 37 °C for 1 h. The incubated samples were plated onto LB agar plates containing 100 µg/mL ampicillin overnight. The confirmed colonies containing the desired plasmid were cultured overnight with LB medium and ampicillin. Plasmid pUC19 was extracted from *E. coli* DH5α using a plasmid extraction kit (MACHEREY-NAGEL, Germany), and the concentration of the purified plasmid was determined by Quantus Fluorometer analysis. Further, the purified plasmid was diluted with sterile deionized water to obtain the ARGs solution and used for adsorption experiments.

Adsorption and desorption experiments—The initial concentration of ARGs was set at 0.01 ng/µL. After 180 minutes of shaking, centrifugation was conducted for 10 minutes at 12,000 g to separate AC particles. The obtained supernatant was subjected to ARGs quantification by quantitative polymerase chain reaction (qPCR). The settled AC was subjected to desorption experiments by adding 1 ml of sterilized deionized water to the settled AC and kept shaking under the same conditions as the adsorption experiments. The concentration of ARGs before and after desorption was also quantified using qPCR analysis. The pseudo-first and pseudo-second-order kinetic models described below were used to analyze the data from the experiments.

$$\frac{dq_t}{dt} = k_1(q_e - q_t) \qquad (1)$$

$$\frac{dq_t}{dt} = k_2(q_e - q_t)^2 \qquad (2)$$

where q_t (copies/mg) is ARG adsorbed onto AC at time t, q_e (copies/mg) is adsorption capacity at equilibrium, k_1 and k_2 (copies.min/mg) are the pseudo-first and pseudo-second-order rate constant, respectively.

RESULTS AND DISCUSSION

Residual concentration of ARGs after adsorption—The residual concentrations of ARGs during contact with different types of AC are displayed in Fig. 1. The rate of adsorption was rapid at the beginning and gradually decreased with increasing contact time until equilibrium was attained within 120 min. To ensure complete equilibrium, the experimental data was quantified up to 180 min. The lowest residual concentration in coal-based and wood-based ACs was obtained from carbon A and H. However, the highest residual concentration was found in carbon B for coal-based ACs and carbon F and G for wood-based ACs. The pore size, pore volume, and surface

chemistry of the AC may contribute to the adsorbability of ARGs.

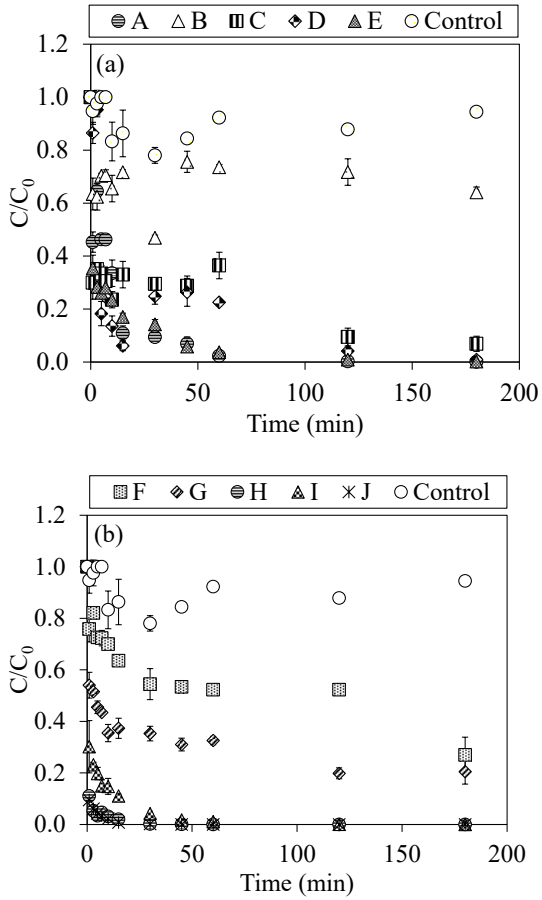

Fig. 1: Residual concentrations of ARGs during contact with (a) coal-based and (b) wood-based ACs (C_0 = 3.4 × 10^{12} copies/L, AC dose = 1 g/L)

Adsorption kinetics of ARGs on different types of AC—Model analysis indicated that the pseudo-second-order kinetic model fitted all experimental data much better than the pseudo-first-order ones as shown in Fig. 2. The R^2 value of the pseudo-second-order was very high (R^2 >0.9699), and the calculated q_e value was in good agreement with the experimental one, suggesting the applicability of the pseudo-second-order kinetic model to describe the adsorption kinetic of ARGs onto AC. This model implies that chemisorption occurs during the adsorption process and the adsorption rate depends on the adsorption capacity, not on the adsorbate concentration.

ARGs concentration after desorption that remains in water—ARG-carrying plasmids were desorbed from ten different types of AC, as illustrated in Fig. 3. The desorbed ARGs from carbon B, F, and G were generally higher than other types of AC. Carbon B, F, and G were highly microporous, with pore volume percentages of 98.1, 96.4, and 90.9 % at pore sizes below 15 Å, respectively. This result indicates that the size exclusion effect prevents ARGs from entering the AC pores below 15 Å, and most ARGs only stick on the external surface of AC, leading to easier desorption into water. This result is also supported by the low adsorption capacity of those ACs (data not shown).

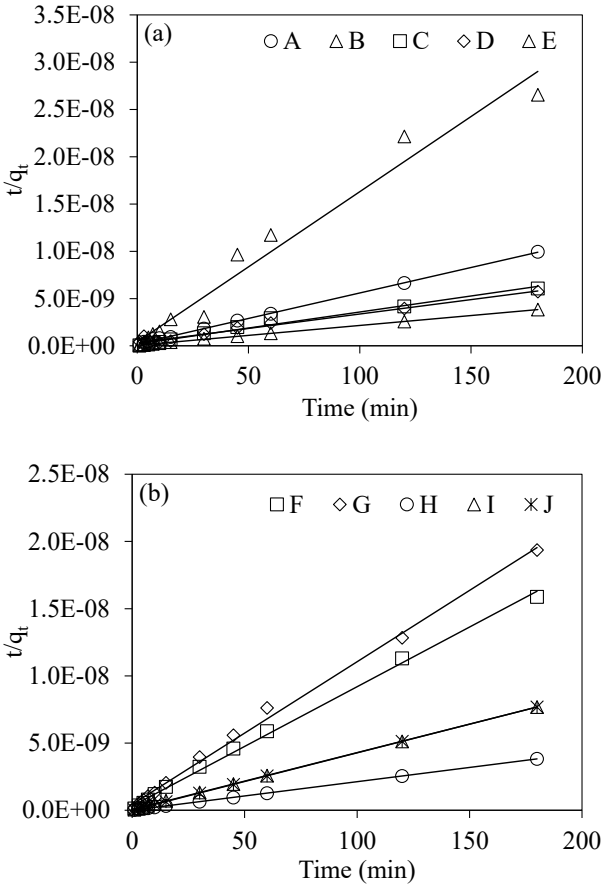

Fig. 2: Pseudo-second-order kinetic models for adsorption of ARGs on (a) coal-based and (b) wood-based ACs (C_0 = 3.4 × 10^{12} copies/L, AC dose = 1 g/L)

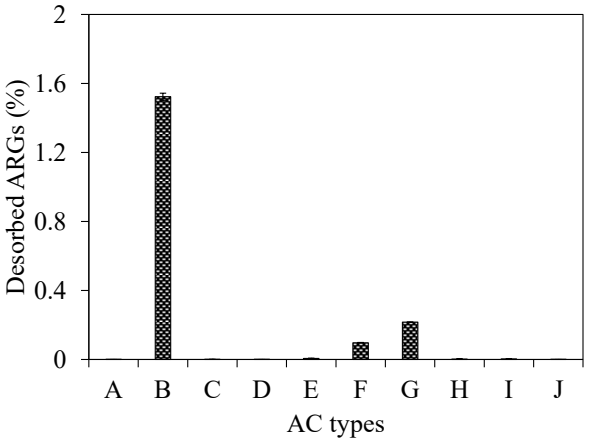

Fig. 3: Desorbed ARGs from different types of AC remaining in water

REFERENCES

Mao D, Luo Y, Mathieu J, Wang Q, Feng L, Mu Q, Feng C and Alvarez PJJ (2014) Persistence of Extracellular DNA in River Sediment Facilitates Antibiotic Resistance Gene Propagation. Environ. Sci. Technol. 48 (1), 71–78.

Proceedings of UGSAS-GU & BWEL
Joint Poster Presentation on Agricultural and
Basin Water Environmental Sciences 2023

Publisher:
The United Graduate School of Agricultural Science,
Gifu University
1-1 Yanagido, Gifu-shi, Gifu 501-1193 Japan

ISBN 978-4-909365-09-5